

REVIEW ARTICLE

Open Access

# Recent advances in functional materials and devices for Zn-Ion hybrid supercapacitors

Weijia Fan<sup>1</sup>, Faxing Wang<sup>2</sup>, Xiaosong Xiong<sup>1</sup>, Bingyan Song<sup>1</sup>, Tao Wang<sup>1</sup>, Xinbing Cheng<sup>1</sup>, Zhi Zhu<sup>1</sup>, Jiarui He<sup>1</sup>, Yankai Liu<sup>3</sup> and Yuping Wu<sup>1</sup> 

## Abstract

Zinc-ion hybrid supercapacitors (ZHSCs) are attracting significant attention due to their high energies/power densities, safety, and low cost. In this review, recent advances in the development of ZHSCs are summarized. Particular emphasis is placed on state-of-the-art cathodes (including carbon, metal oxides, MXenes, and redox-active polymers), anodes (including Zn-based composites and Zn-free materials) and electrolytes for ZHSCs. Furthermore, the latest research on functional ZHSC devices with miniaturized ZHSCs, fiber-shaped ZHSCs, self-chargeable ZHSCs and self-healing devices is reported. Finally, further developments with ZHSCs are envisaged for future research in this thriving field.

## Introduction

With the popularity and use of smart grids and electric vehicles, the demand for energy storage devices with high energy and power densities, excellent safety, and long cycling lives is increasing<sup>1,2</sup>. Rechargeable batteries and supercapacitors are widely researched and have been used for commercial applications<sup>3–5</sup>. Rechargeable batteries consist of two battery-type electrodes that store energy through redox reactions, such as ion intercalation/deintercalation, phase transformations, or stripping/plating at the anode and cathode; these batteries typically have very high energy densities and are mainly used in portable electronics and electric vehicles. However, the redox reactions in rechargeable batteries usually lead to short cycling lives and low power densities owing to volume variations and sluggish kinetics. Supercapacitors consist of two capacitive electrodes that store and convert energy through electrochemical double-layer capacitive or pseudocapacitive behavior; therefore, supercapacitors have high power densities and are used mainly in consumer

electronics, backup power sources, renewable energy generation systems, rail transportation, military equipment, aerospace, and other fields, etc. However, the energy densities of supercapacitors are insufficient and need to be increased. For this reason, the concept of hybrid supercapacitors was developed. Hybrid supercapacitors combine the advantages of both batteries and supercapacitors by using capacitive and battery-type materials as electrodes. During charging and discharging, the capacitive electrodes serve as electrochemical double-layer capacitors or pseudocapacitors, and the battery-type electrodes carry out redox reactions (Fig. 1)<sup>5,6</sup>. When constructing hybrid supercapacitors, it is necessary to ensure that the supercapacitors have capacitive electrodes and battery-type electrodes. That is, hybrid supercapacitors can be classified into two types: one has a capacitor-type cathode and a battery-type anode; the other, on the contrary, has a battery-type cathode and a capacitor-type anode.

Among the various hybrid supercapacitors, nonaqueous lithium-ion hybrid capacitors were demonstrated early. However, considering the scarcity and safety issues associated with lithium resources and organic electrolytes, researchers have started to explore the prospects of other ion hybrid capacitors because of their lower costs and safety. Zinc (Zn) is very promising due to its high

Correspondence: Faxing Wang ([faxingwang11@fudan.edu.cn](mailto:faxingwang11@fudan.edu.cn)) or Yuping Wu ([wuyup@fudan.edu.cn](mailto:wuyup@fudan.edu.cn))

<sup>1</sup>School of Energy and Environment, Southeast University, 210096 Nanjing, China

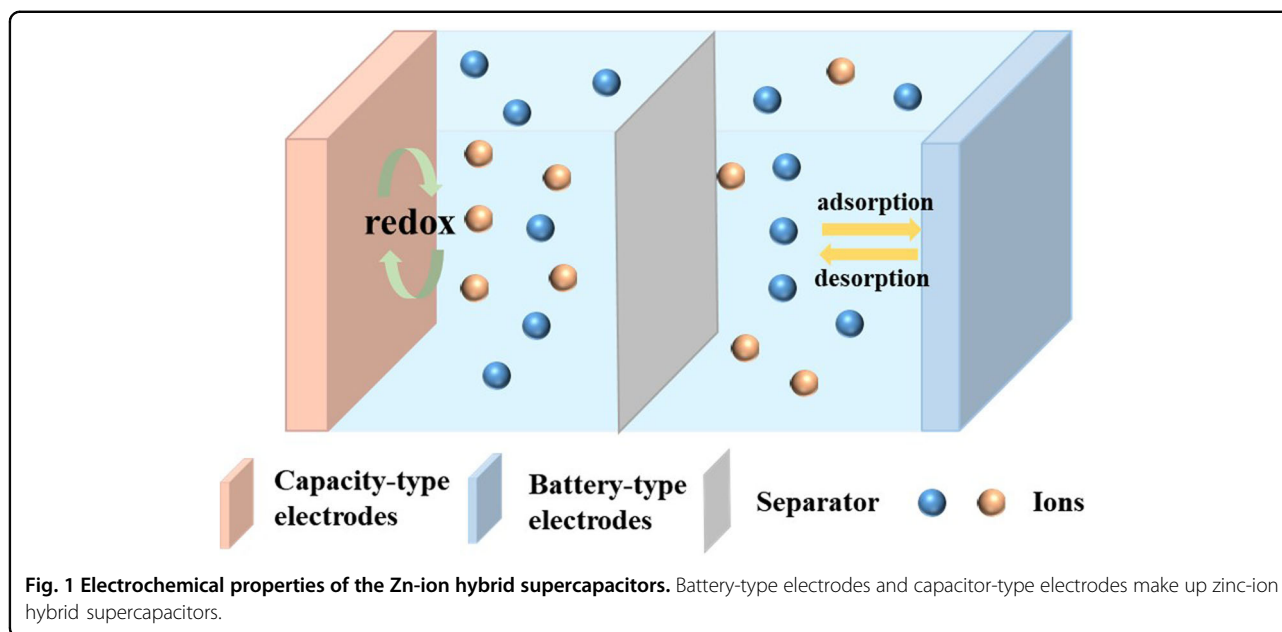
<sup>2</sup>Center for Advancing Electronics Dresden, Technische Universität Dresden, 01069 Dresden, Germany

Full list of author information is available at the end of the article

© The Author(s) 2024



**Open Access** This article is licensed under a Creative Commons Attribution 4.0 International License, which permits use, sharing, adaptation, distribution and reproduction in any medium or format, as long as you give appropriate credit to the original author(s) and the source, provide a link to the Creative Commons licence, and indicate if changes were made. The images or other third party material in this article are included in the article's Creative Commons licence, unless indicated otherwise in a credit line to the material. If material is not included in the article's Creative Commons licence and your intended use is not permitted by statutory regulation or exceeds the permitted use, you will need to obtain permission directly from the copyright holder. To view a copy of this licence, visit <http://creativecommons.org/licenses/by/4.0/>.



theoretical capacity ( $820 \text{ mAh g}^{-1}$ ), low redox potential ( $-0.76 \text{ V}$  vs. the standard hydrogen electrode (SHE)) and high reliability. Therefore, zinc-ion hybrid capacitors (ZHSCs), which combine the advantages of Zn-ion batteries, such as low cost, environmental friendliness, and low redox potentials of the Zn anodes, and the advantages of supercapacitors, including fast charge–discharge rates, high power densities and long cycling lives, show attractive application prospects. Conventional ZHSCs use conventional carbon materials as the cathodes, commercial Zn foils as the anodes, and aqueous Zn salts as the electrolytes. Conventional carbon materials, such as activated carbon (AC), exhibit capacitive properties, but their limited specific capacitance cannot be matched with those of Zn anodes with high capacities, resulting in a waste of resources<sup>7,8</sup>. On the anode side, the need to polish the surface oxide layer of commercial Zn foil may cause fine traces to form on the surface of the Zn foil, leading to the formation of dendrites during cycling, which can affect the cycling life<sup>9–11</sup>. In addition, the interactions between water molecules and the anions in water-soluble Zn salts ( $\text{ZnCl}_2$ ,  $\text{ZnSO}_4$ ,  $\text{Zn}(\text{CF}_3\text{SO}_3)_2$ , and  $\text{Zn}(\text{CH}_3\text{COO})_2$ ) can affect ion adsorption/desorption or deposition/exfoliation, which may cause a range of issues, such as byproduct formation and the hydrogen evolution reaction<sup>12,13</sup>. Here, we present the latest cathode and anode materials, compare the effects of advanced electrolytes on the performance of ZHSCs, and summarize the prospects for application of new ZHSCs. Moreover, novel design strategies for functional ZHSC devices are highlighted. In addition, we provide our perspectives on the remaining challenges and future research opportunities for the development of electrode materials, electrolytes, and devices for ZHSCs.

### Functional cathode materials

In ZHSCs, the cathode is a crucial component. The development of new cathode materials with high electrical conductivities and large specific capacities is the most effective approach to increasing the energy densities and power densities of ZHSCs. Currently, potential candidate materials for ZHSCs include three-dimensional (3D) carbon, metal oxides, MXenes, redox-active polymers, and other cathode materials. All of the performance metrics are benchmarked in Table 1.

### 3D carbon

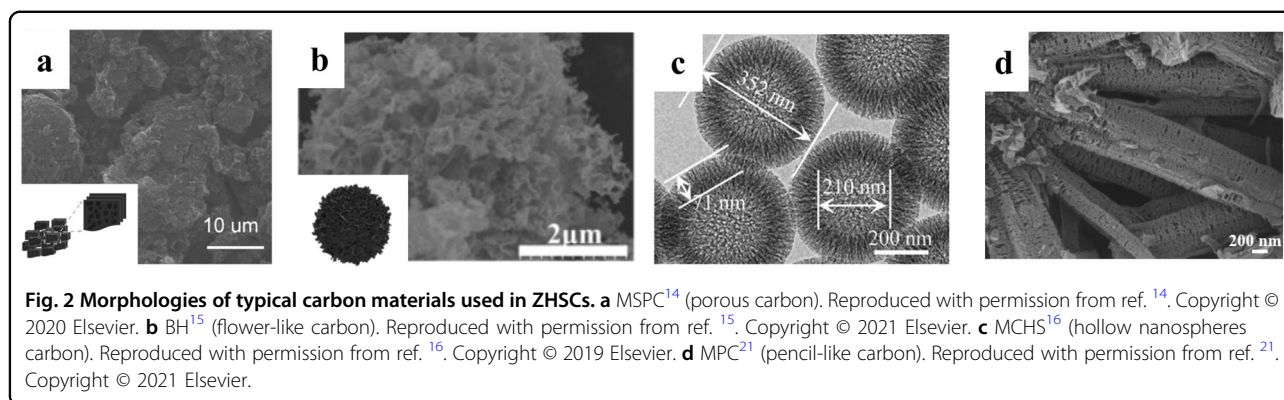
Carbon materials are among the most common electrode materials used in supercapacitors due to their large specific surface areas, high electrical conductivities, and tunable porosities. Early aqueous ZHSCs were prepared with AC as the cathode, Zn as the anode, and a  $\text{ZnSO}_4$  aqueous solution as the electrolyte<sup>7</sup>. The assembled ZHSCs exhibited high specific capacities ( $121 \text{ mAh g}^{-1}$  at  $0.1 \text{ A g}^{-1}$ ) and excellent cycling lives. It is well known that electrochemical double-layer capacitive behavior depends on the specific surface area; therefore, carbonaceous materials with various morphologies have been explored to optimize their electrochemical properties. Porous carbon has been widely studied as a cathode material in ZHSCs due to its mature synthetic methods and tunable nature. For example, porous carbon was developed as a high-performance cathode for ZHSCs by the molten salt method using bitumen as the carbon source and was denoted as a porous carbon assisted by molten salt carbonization (MSPC) (Fig. 2a)<sup>14</sup>. The prepared MSPCs had high specific surface areas ( $499.3 \text{ m}^2 \text{ g}^{-1}$ ) and abundant mesopores, which provided highly active sites and

**Table 1 Comparison of the properties of various cathode materials.**

Cathode	Specific surface area ( $\text{m}^2 \text{g}^{-1}$ )	Anode	Electrolyte	Voltage Window (V)	Capacity or capacitance	Cycling stability	Ref.
AC	1923	Zn	ZnSO <sub>4</sub>	0.2–1.8	121 mAh g <sup>-1</sup> (0.1 A g <sup>-1</sup> )	91% after 10,000 cycles (1 A g <sup>-1</sup> )	7
RNP-1-2-Air	93	Zn	ZnSO <sub>4</sub>	0.2–1.8	215.2 F g <sup>-1</sup> (0.1 A g <sup>-1</sup> )	~100% after 10,000 cycles (5 A g <sup>-1</sup> )	19
MPC-2	2125	Zn	Zn(CF <sub>3</sub> SO <sub>3</sub> ) <sub>2</sub>	0–1.8	289.2 F g <sup>-1</sup> (0.2 A g <sup>-1</sup> )	96.7% after 10,000 cycles (10 A g <sup>-1</sup> )	21
HHT-rGO	197.2	Zn	ZnSO <sub>4</sub>	0–1.6	277 F g <sup>-1</sup> (0.2 A g <sup>-1</sup> )	97.8% after 20,000 cycles (2.5 A g <sup>-1</sup> )	22
PN-CHONS	297	Zn In	ZnSO <sub>4</sub>	0.2–1.8	164.4 mAh g <sup>-1</sup> (0.2 A g <sup>-1</sup> )	80.6% after 12,000 cycles (2.5 A g <sup>-1</sup> )	18
NSPCs	1385	Zn	Zn(CF <sub>3</sub> SO <sub>3</sub> ) <sub>2</sub>	0–1.8	262.7 F g <sup>-1</sup> (0.05 A g <sup>-1</sup> )	99.5% after 15,000 cycles (2.5 A g <sup>-1</sup> )	17
CT/SWNT	947	Zn	ZnSO <sub>4</sub>	0.2–1.8	127.6 mAh g <sup>-1</sup> (0.1 A g <sup>-1</sup> )	90% after 10,000 cycles (5 A g <sup>-1</sup> )	20
MSPC	499.3	Zn	ZnSO <sub>4</sub>	0–1.8	127.6 mAh g <sup>-1</sup> (0.68 A g <sup>-1</sup> )	85.4% after 10,000 cycles (5.44 A g <sup>-1</sup> )	14
BH	1076	Zn	ZnSO <sub>4</sub>	0–1.8	132 mAh g <sup>-1</sup> (1 A g <sup>-1</sup> )	10,000 cycles (5 A g <sup>-1</sup> )	15
HCSs	819.5	Zn deposited on carbon cloth	ZnSO <sub>4</sub> + polyacrylamide (PAM)	0.2–1.8	86.8 mAh g <sup>-1</sup> (0.5 A g <sup>-1</sup> )	98% after 15,000 cycles (1 A g <sup>-1</sup> )	79
MnO <sub>2</sub>	/	AC	ZnSO <sub>4</sub> + MnSO <sub>4</sub>	0–2	83.8 mAh g <sup>-1</sup> (0.1 A g <sup>-1</sup> )	91% after 4500 cycles (1 A g <sup>-1</sup> )	25
Zn <sub>x</sub> MnO <sub>2</sub>	/	Activated carbon cloth	ZnSO <sub>4</sub> + MnSO <sub>4</sub>	0–2	1745.8 mF cm <sup>-2</sup> (2 mA cm <sup>-2</sup> )	83.1% after 5000 cycles (15 A g <sup>-1</sup> )	28
MnO <sub>2</sub> -CNTs	/	MXene (Ti <sub>3</sub> C <sub>2</sub> T <sub>x</sub> )	ZnSO <sub>4</sub> + MnSO <sub>4</sub>	0–0.8	115.1 F g <sup>-1</sup> (1 mV s <sup>-1</sup> )	83.6% after 15,000 cycles (5.244 A g <sup>-1</sup> )	26
V <sub>2</sub> O <sub>5</sub>	/	Ti <sub>3</sub> C <sub>2</sub> T <sub>x</sub>	ZnSO <sub>4</sub> + PAM	0–1.65	129 mF cm <sup>-2</sup> (0.34 mA cm <sup>-2</sup> )	98% after 10,000 cycles (2.30 mA cm <sup>-2</sup> )	29
Co <sub>9</sub> S <sub>8</sub> @MnO <sub>2</sub>	/	Zn	ZnSO <sub>4</sub>	0–2.6	2.094 F cm <sup>-2</sup> (5 mA cm <sup>-2</sup> )	86% after 5000 cycles (5 mA cm <sup>-2</sup> )	27
RuO <sub>2</sub> ·H <sub>2</sub> O	57	Zn	Zn(CF <sub>3</sub> SO <sub>3</sub> ) <sub>2</sub>	0.4–1.6	122 mAh g <sup>-1</sup> (0.1 A g <sup>-1</sup> )	87.5% after 10,000 cycles (20 A g <sup>-1</sup> )	23

Table 1 continued

Cathode	Specific surface area ( $\text{m}^2 \text{g}^{-1}$ )	Anode	Electrolyte	Voltage Window (V)	Capacity or capacitance	Cycling stability	Ref.
MXene-rGO	/	Zn	ZnSO <sub>4</sub>	0.2–1.6	128.6 F $\text{cm}^{-2}$ (0.4 A $\text{g}^{-1}$ )	95% after 7000 cycles (5 A $\text{g}^{-1}$ )	110
Ti <sub>3</sub> C <sub>2</sub>	/	Zn	ZnSO <sub>4</sub>	0.1 – 1.35	132 F $\text{g}^{-1}$ (0.5 A $\text{g}^{-1}$ )	82.5% after 1000 cycles (5 A $\text{g}^{-1}$ )	30
EE-Ti <sub>3</sub> C <sub>2</sub> T <sub>x</sub>	/	Zn	ZnSO <sub>4</sub> + PAM	0.2–1.6	239.1 F $\text{g}^{-1}$ (0.5 mA $\text{cm}^{-2}$ )	/	32
Ti <sub>3</sub> C <sub>2</sub> T <sub>x</sub>	/	Zn	ZnSO <sub>4</sub> + PAM	0.1–1.2	318 $\mu\text{F cm}^{-2}$ (5 mV $\text{s}^{-1}$ ),	76% after 10,000 cycles (20 $\mu\text{A cm}^{-2}$ )	111
Ti <sub>3</sub> C <sub>2</sub>	/	3DP CNT/Zn	ZnSO <sub>4</sub>	0.1–1.2	1006.4 mF $\text{cm}^{-2}$ (0.5 mA $\text{cm}^{-2}$ )	86.5% after 16,000 cycles (10 mA $\text{cm}^{-2}$ )	33
3D-PHMF	107	Zn	Zn(CF <sub>3</sub> SO <sub>3</sub> ) <sub>2</sub>	0–1.3	105.6 mAh $\text{g}^{-1}$ (0.2 A $\text{g}^{-1}$ )	90% after 20,000 cycles (5 A $\text{g}^{-1}$ )	35
N- Ti <sub>3</sub> C <sub>2</sub>	2795	Zn	ZnSO <sub>4</sub>	0.05–1.2	247.9 F $\text{g}^{-1}$ (0.1 A $\text{g}^{-1}$ )	88.34% after 6000 cycles (1.5 A $\text{g}^{-1}$ )	34
Sn <sup>4+</sup> -Ti <sub>2</sub> CT <sub>x</sub> /C	64	Zn@CC	LiTFSI + Zn(OTf) <sub>2</sub> + PAM	0.1–2	138 mAh $\text{g}^{-1}$ (0.1 A $\text{g}^{-1}$ )	95% after 12,500 cycles (0.5 A $\text{g}^{-1}$ )	36
Ti <sub>3</sub> C <sub>2</sub> T <sub>x</sub> /Bi <sub>2</sub> S <sub>3</sub> @N-C	/	Zn	ZnSO <sub>4</sub>	0–1.5	150.33 F $\text{g}^{-1}$ (1 A $\text{g}^{-1}$ )	85.71% after 2000 cycles (53 A $\text{g}^{-1}$ )	37
PDA@PCC	/	Zn	ZnSO <sub>4</sub>	0.1–1.8	1.25 mAh $\text{cm}^{-2}$ (1 mA $\text{cm}^{-2}$ )	100% after 10,000 cycles (10 mA $\text{cm}^{-2}$ )	38
PA-COF	196	Zn	ZnSO <sub>4</sub>	0.2–1.6	247 mAh $\text{g}^{-1}$ (0.1 A $\text{g}^{-1}$ )	99.62% after 10,000 cycles (1 A $\text{g}^{-1}$ )	39
poly(4,4'-thiophenol)/AC	1820	Zn	ZnSO <sub>4</sub>	0.1–1.9	0.38 mAh $\text{cm}^{-2}$ (0.3 A $\text{g}^{-1}$ )	74% after 2000 cycles	40
TiN	/	Zn	ZnSO <sub>4</sub> /Zn(Ac) <sub>2</sub> /ZnCl <sub>2</sub>	0.1–1.9	489.8 F $\text{g}^{-1}$ (0.2 A $\text{g}^{-1}$ )	84.6% after 6700 h (0.2 A $\text{g}^{-1}$ )	43
FL-P	/	Zn	LiTFSI + Zn(CF <sub>3</sub> SO <sub>3</sub> ) <sub>2</sub> / ZnCl <sub>2</sub> + Et <sub>4</sub> NBF <sub>4</sub> / PC	0.8–2.2/0.8–2.5	304 F $\text{g}^{-1}$ (0.2 A $\text{g}^{-1}$ )/363.9 F $\text{g}^{-1}$ (0.2 A $\text{g}^{-1}$ )	/	42
Few-layer siloxane	1986	Zn	LiTFSI+Zn(CF <sub>3</sub> SO <sub>3</sub> ) <sub>2</sub>	0–1.8	6.58 mF $\text{cm}^{-2}$ (0.05 mA $\text{cm}^{-2}$ )	94.3% after 16,000 cycles	41



facilitated ion transport. In addition to porous carbon, flower-like carbons with increased specific surface areas and hydrogen-bonded frameworks (HOFs) were rapidly synthesized by recrystallization at room temperature<sup>15</sup>. Heavy fractions of bio-oil were encapsulated in HOFs to obtain bio-oil@HOF (BH) composites, which were carbonized to prepare carbon materials (Fig. 2b). Due to the high utilization of active sites, the ZHSCs exhibited energy densities of up to  $117.5 \text{ Wh kg}^{-1}$  at  $890 \text{ W kg}^{-1}$  and maintained  $60.7 \text{ Wh kg}^{-1}$  even at  $16.2 \text{ kW kg}^{-1}$ . Another example is hollow carbon nanospheres. The hollow structures of these materials expand the contact area between the electrolyte and the electrode, increasing the energy density. To obtain mesoporous carbon hollow spheres (MCHSs), synthetic phenolic resins and pore-forming particles were coated onto tetrapropylorthosilicate templates to form  $\text{SiO}_2@\text{SiO}_2/\text{RF}$  core-shell structures, which were subsequently carbonized, after which the template was removed (Fig. 2c)<sup>16</sup>. As a cathode material, mesoporous hollow carbon spheres have been demonstrated to have excellent electrochemical performance.

The properties of carbon materials can also be enhanced by doping with other elements. N,S-codoped porous carbons (NSPCs) with well-developed pores and large surface areas were synthesized via coactivation<sup>17</sup>. Their unique interconnected lamellar structures with cavities provided many pathways for electron transport and abundant channels for rapid ion transport. More importantly, the introduction of N and S heteroatoms provided additional active sites for ion adsorption. In addition,  $\text{MnO}_2$  nanoflowers were used as bifunctional templates to form P/N dual-doped hollow nanospheres (PN-CHoNS) after induced carbonization<sup>18</sup>. The 3D porous structures shortened the ion transport paths, the hollow structures enabled fast kinetics and smaller volume changes, and P/N dual doping enhanced the adsorption of Zn ions. Thus, ZHSCs based on the PN-CHoNS cathode had high energy densities of  $116.0 \text{ Wh kg}^{-1}$  and high power densities of

$21,660 \text{ W kg}^{-1}$ . Similarly, N, P, and O codoped carbon materials (RNP-1-2-Air) were prepared by combining air plasma treatment with N, P, and O codoping<sup>19</sup>. The plasma treatment increased the hydrophilicities of the prepared materials. Moreover, N, P, and O codoping was used to adjust the functional and electronic properties of carbon microspheres. In a similar vein, cottonwood-derived quasi-two-dimensional tile-shaped carbon sheets (denoted as carbon tile, CT) were developed<sup>20</sup>. The large specific surface areas, proper curvature, thin walls, and multifunctional doping (O, P, N) provided short ion penetration paths, ensured fast ion diffusion, and improved electron transport efficiency. In general, doping carbon cathodes with heteroatoms such as N and P increased the pseudocapacitance by enhancing the chemisorption of Zn ions.

Electronegative oxygenated groups can reduce the Zn-ion adsorption barrier and form an electrostatic electrochemical double-layer capacitance, thereby improving the electrochemical double-layer capacitance. Moreover, similar to N and S dopants, oxygen functional groups provided additional pseudocapacitance by introducing a rapid redox reaction on/near the carbon surface and making the electrodes more hydrophilic. Therefore, the introduction of surface redox groups increased the number of adsorption sites and provided additional redox pseudocapacitance. To obtain sharpened pencil-like nanoporous carbon (MPC) with a high specific surface area, hierarchical porous structure, and numerous oxygen functional groups, a metal-organic framework (MOF) was used as a precursor in combination with chemical activation methods (Fig. 2d)<sup>21</sup>. Assembled ZHSC devices achieved high energy densities of up to  $130.1 \text{ Wh kg}^{-1}$  at a power output of  $180.3 \text{ W kg}^{-1}$ . At a maximum power density of  $7.8 \text{ kW kg}^{-1}$ , a high energy density of  $56 \text{ Wh kg}^{-1}$  was still provided. However, these oxygen functional groups with structural defects significantly reduced the electrical conductivity of the carbon material, which also seriously affected the specific capacitance. Accordingly, it is extremely important to optimize the rGO reasonably<sup>22</sup>.

It was found that rGO produced by modulating the oxygen functional groups exhibited excellent electrochemical properties, and the assembled quasisolid flexible ZHSCs increased the areal energy density to  $342 \mu\text{W h cm}^{-2}$ . The carboxyl and carbonyl groups also significantly improved the aqueous electrolyte wettability, Zn-ion chemisorption, and pseudocapacitive redox activities.

Generally, carbon materials offer great promise in the development of ZHSCs due to their diverse structures, large specific surface areas, and mature synthetic methods. Increases in the specific surface areas, while increasing the capacitance, also affect charge storage and the cycling life. Future research should be focused on modulating the pore sizes and synthesizing ordered structures to regulate the specific surface area, as well as improving the electrochemical properties through doping with heteroatoms and introducing functional groups. Based on an understanding of the pore sizes and pore shapes of carbon materials in supercapacitors, the optimal pore size would be twice the radius of the solvated ions, which would increase the capacitance.

#### Transitional metal oxides

Transition metal oxides (TMOs) have high specific capacitances ( $100\text{--}2000 \text{ F g}^{-1}$ ) and excellent chemical stabilities and are therefore widely used as new cathode materials in ZHSCs.

$\text{RuO}_2$  has a high theoretical capacitance ( $2000 \text{ F g}^{-1}$ ) and fast faradaic redox reactions, good electrical conductivity, high chemical and thermal stability, and a large voltage window.  $\text{RuO}_2$  is therefore a most ideal cathode material for pseudocapacitive charge storage. Amorphous  $\text{RuO}_2 \cdot \text{H}_2\text{O}$  was first used in the cathodes for ZHSCs and assembled ZHSCs based on a pseudocapacitive storage mechanism to achieve fast charging/discharging rates (36 s), high energy densities ( $82 \text{ Wh kg}^{-1}$ ), and ultralong lifetimes (10,000 cycles). Kinetic analyses indicated that ultrafast  $\text{Zn}^{2+}$  storage in the  $\text{RuO}_2 \cdot \text{H}_2\text{O}$  cathode originated from a redox reaction<sup>23</sup>. Furthermore, the structural water in  $\text{RuO}_2 \cdot \text{H}_2\text{O}$  played a crucial role in the storage of  $\text{Zn}^{2+}$ . By comparing anhydrous  $\text{RuO}_2$  and  $\text{RuO}_2 \cdot \text{H}_2\text{O}$ , it was found that although anhydrous  $\text{RuO}_2$  typically has a higher electrical conductivity than aqueous  $\text{RuO}_2 \cdot \text{H}_2\text{O}$ , the redox pseudocapacitance reaction was significantly suppressed in anhydrous  $\text{RuO}_2$ .

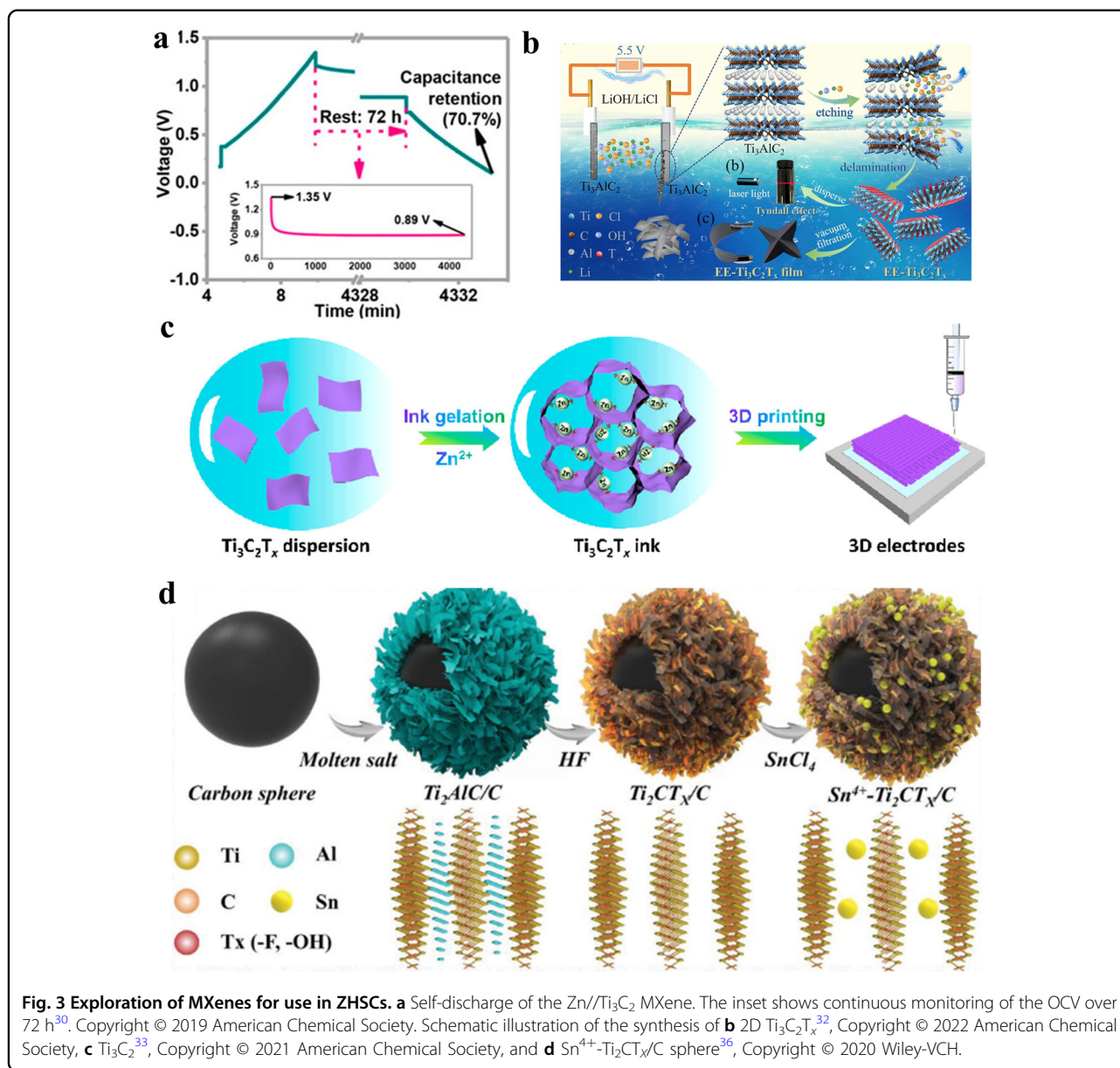
Materials such as manganese oxides, vanadium oxides, and Prussian blue analogs were used as cathodes in Zn-ion batteries<sup>9,10,24</sup>. These unique materials provided inspiration for the design of battery-type cathodes in which Zn ions were inserted/extracted for ZHSCs. Among these materials, manganese-based oxides offered unique advantages, such as abundant resources, low toxicities, and low costs, endowing them with the potential for use as battery-type cathode materials for

ZHSCs.  $\text{MnO}_2$ , AC, and  $\text{ZnSO}_4$  were used as the cathodes, anodes, and electrolytes, respectively, of ZHSCs<sup>25</sup>. The ion storage mechanism, i.e., reversible insertion/extraction of  $\text{Zn}^{2+}$  in  $\text{MnO}_2$  nanorods, ionic adsorption/desorption on the surface of AC particles, and partially reversible formation/dissolution of the byproduct  $\text{Zn}_4(\text{OH})_6\text{SO}_4 \cdot n\text{H}_2\text{O}$ , was investigated. The electrolyte was then optimized to suppress the formation of byproducts and the dissolution of manganese. Interestingly, the addition of  $\text{Mn}^{2+}$  gave an increase in the energy density, while the replacement of  $\text{ZnSO}_4$  with  $\text{Zn}(\text{CF}_3\text{SO}_3)_2$  alleviated both problems. However, the relatively low electrical conductivity and structural collapse during cycling severely limited the reaction kinetics and reduced the structural stability of  $\text{MnO}_2$ .  $\text{MnO}_2$  and CNTs were combined to obtain  $\text{MnO}_2$ -CNT with a higher electrical conductivity<sup>26</sup>. In contrast, a core-shell heterostructured  $\text{Co}_9\text{S}_8@ \text{MnO}_2$  cathode with tunable oxygen vacancies was constructed<sup>27</sup>. Due to the  $\text{Co}_9\text{S}_8$  nanotube arrays and the presence of oxygen vacancies, electron transport through the interface was facilitated; this provided a larger surface area, increased the intrinsic electrical conductivity of  $\text{MnO}_2$ , and increased the electrochemically active area. As a result, the assembled ZHSCs exhibited excellent electrochemical properties. XRD also revealed that protons were reversibly intercalated and extracted in  $\text{Co}_9\text{S}_8@ \text{MnO}_2$  during cycling. In addition,  $\text{Zn}_x\text{MnO}_2$  was grown on carbon cloth by  $\text{Zn}^{2+}$  preembedding<sup>28</sup>. Zn-ion preintercalation improved the stabilities of the manganese-based cathodes, and the assembled ZHSCs maintained 83.1% of the initial capacity after 5000 cycles at  $15 \text{ mA cm}^{-2}$ , far exceeding the efficiencies of  $\text{MnO}_2$ -based ZHSCs (45.3% capacitance retention after 5000 cycles at  $15 \text{ mA cm}^{-2}$ ).

Due to its high theoretical capacity based on multiple electron transfers ( $589 \text{ mAh g}^{-1}$ ),  $\text{V}_2\text{O}_5$  shows great potential as a cathode material for ZHSCs. Thus, new ZHSCs with  $\text{V}_2\text{O}_5$  as the battery-type cathodes were designed<sup>29</sup>. As expected, the ZHSCs exhibited good electrochemical performance with high area capacitances ( $129 \text{ mF cm}^{-2}$ ) and high energy densities ( $48.9 \mu\text{Wh cm}^{-2}$ ). However, the areal power densities of ZHSCs with  $\text{V}_2\text{O}_5$  cathodes were still inferior to those of ZHSCs with capacitive or pseudocapacitive cathodes owing to the sluggish kinetics of battery-type redox reactions.

#### MXenes

MXene materials constitute another class of cathode materials for ZHSCs because of their graphene-like two-dimensional (2D) layer structures, excellent metallic conductivities, high hydrophilicities, superior mechanical strengths, and large numbers of surface pseudocapacitance charge storage sites.  $\text{Ti}_3\text{C}_2$  MXene was obtained by HF removal of Al from the layered  $\text{Ti}_3\text{AlC}_2$  precursor



followed by centrifugation and vacuum filtration. Ti<sub>3</sub>C<sub>2</sub> MXene and Zn nanosheets were assembled to form degradable rechargeable ZHSCs with excellent resistance to self-discharge, and Zn nanosheets were obtained by the deposition of Zn on Ti<sub>3</sub>C<sub>2</sub><sup>30</sup>. The assembled ZHSCs stored/converted electrical energy via ion adsorption/desorption on the Ti<sub>3</sub>C<sub>2</sub> MXene cathodes and deposition/exfoliation of Zn<sup>2+</sup> on the Zn anodes. Over 82% of the capacitance was maintained after 1000 cycles. Notably, the assembled capacitors exhibited minimum self-discharge rates of 6.4 mV h<sup>-1</sup> (Fig. 3a) and were completely degraded in phosphate-buffered saline within 7.5 days. In addition, Ti<sub>3</sub>C<sub>2</sub>T<sub>x</sub>/nanofibrillated cellulose (NFC) was obtained by LiF/HCl etching and alkylation of

Ti<sub>3</sub>C<sub>2</sub>T<sub>x</sub> complexed with NFC<sup>31</sup>. Due to the presence of NFCs, which suppressed aggregation problems and increased electrolyte contact, the assembled ZHSCs exhibited large specific capacities (92.1 mAh g<sup>-1</sup>, 0.5 mA cm<sup>-2</sup>) and excellent cycling stabilities (94.31% capacity retention after 10,000 cycles at 8 mA cm<sup>-2</sup>).

The abovementioned synthetic methods for MXene materials required F-based reagents (HF, LiF/HCl, etc.). These methods are time-consuming and present safety hazards. Moreover, F-based etching methods can create F-terminal functional groups on the MXene surface that impede the transport of electrolyte ions and reduce the number of electroactive sites, thus decreasing the electrochemical performance. Hence, Ti<sub>3</sub>C<sub>2</sub>T<sub>x</sub> was etched

with a simple, time-saving fluorine-free electrochemical method (Fig. 3b)<sup>32</sup>. Additionally, layered  $\text{Ti}_3\text{C}_2\text{T}_x$  was obtained directly after sonication and without the use of any hazardous organic embedding agents. Flexible quasi-solid ZHSCs were constructed that provided large area energy densities of 249.9 and 199.1  $\mu\text{Wh cm}^{-2}$  at power densities of 312.4 and 6471  $\mu\text{W cm}^{-2}$ , respectively. Moreover, additive-free  $\text{Ti}_3\text{C}_2$  MXene inks were prepared via a divalent cation-assisted gelation strategy, and the 3D-printed  $\text{Ti}_3\text{C}_2$  MXene was used in ZHSCs<sup>33</sup> (Fig. 3c). The  $\text{Ti}_3\text{C}_2$  MXene electrodes were systematically investigated with in situ/ex situ methods to reveal a dual ion storage mechanism, i.e., pseudocapacitive behavior for  $\text{H}^+$  and bilayer capacitive behavior for  $\text{Zn}^{2+}$ . Impressively, excellent rate performance of the 3D-printed MXene cathode (184.4  $\text{F g}^{-1}$  at 10  $\text{A g}^{-1}$ ) was achieved.

However, restacking and agglomeration of the MXene layers can lead to a loss of electrochemically active sites and slow penetration of the electrolyte. Interestingly, the insertion of other substances on the surfaces or between the layers of MXene prevented restacking. After obtaining the  $\text{Ti}_3\text{AlC}_2$  phase by chemical etching, N- $\text{Ti}_3\text{C}_2$  was also synthesized by a one-step hydrothermal method using urea as the nitrogen source<sup>34</sup>. The introduced nitrogen heteroatoms increased the interlayer repulsion, suppressed self-aggregation of the  $\text{Ti}_3\text{C}_2$  sheets, and improved the structural stability of  $\text{Ti}_3\text{C}_2$ . A 3D porous H-MXene film (3D-PHMF) was constructed via a reduced rejection and freeze-casting assembly method<sup>35</sup>. Compared to the MXene film and 3D-porous MXene film, the as-prepared 3D-PHMF had a larger specific surface area. The abundant pores provided larger surface areas with abundant active sites for  $\text{Zn}^{2+}$  storage, and together with the introduction of  $\text{H}^+$ , electrostatic repulsion between the weakened layers was attenuated, and the assembled ZHSC exhibited remarkable cycling stability for up to 20,000 cycles. Similarly, Sn- $\text{Ti}_2\text{CT}_x/\text{C}$  spherical cathodes were obtained by inserting  $\text{Sn}^{4+}$  into  $\text{Ti}_2\text{CT}_x$  after distributing MXene sheets vertically on the outer surfaces of the carbon spheres in a highly ordered manner (Fig. 3d)<sup>36</sup>. Due to the presence of  $\text{Sn}^{4+}$ , the layer spacing was expanded, and the ion diffusion kinetics were optimized. The assembled ZHSCs exhibited extremely long cycle lives (12,500 cycles at 0.5  $\text{A g}^{-1}$ ). In addition, a new pizza-like ternary heterostructure,  $\text{Ti}_3\text{C}_2\text{T}_x/\text{Bi}_2\text{S}_3@\text{NC}$ , was recently reported<sup>37</sup>. The synergistic interactions among the three components ( $\text{Ti}_3\text{C}_2\text{T}_x$ ,  $\text{Bi}_2\text{S}_3$ , and NC) increased the number of active sites and stabilized the overall structure. Consequently,  $\text{Zn}/\text{Ti}_3\text{C}_2\text{T}_x/\text{Bi}_2\text{S}_3@\text{NC}$  exhibited a high specific capacitance (653  $\text{F g}^{-1}$ ).

The high electrical conductivity and layered structure of MXenes provided ZHSCs with excellent rate performance. Increasing the contact between the electrolyte and electrode by constructing pores on the surface of the

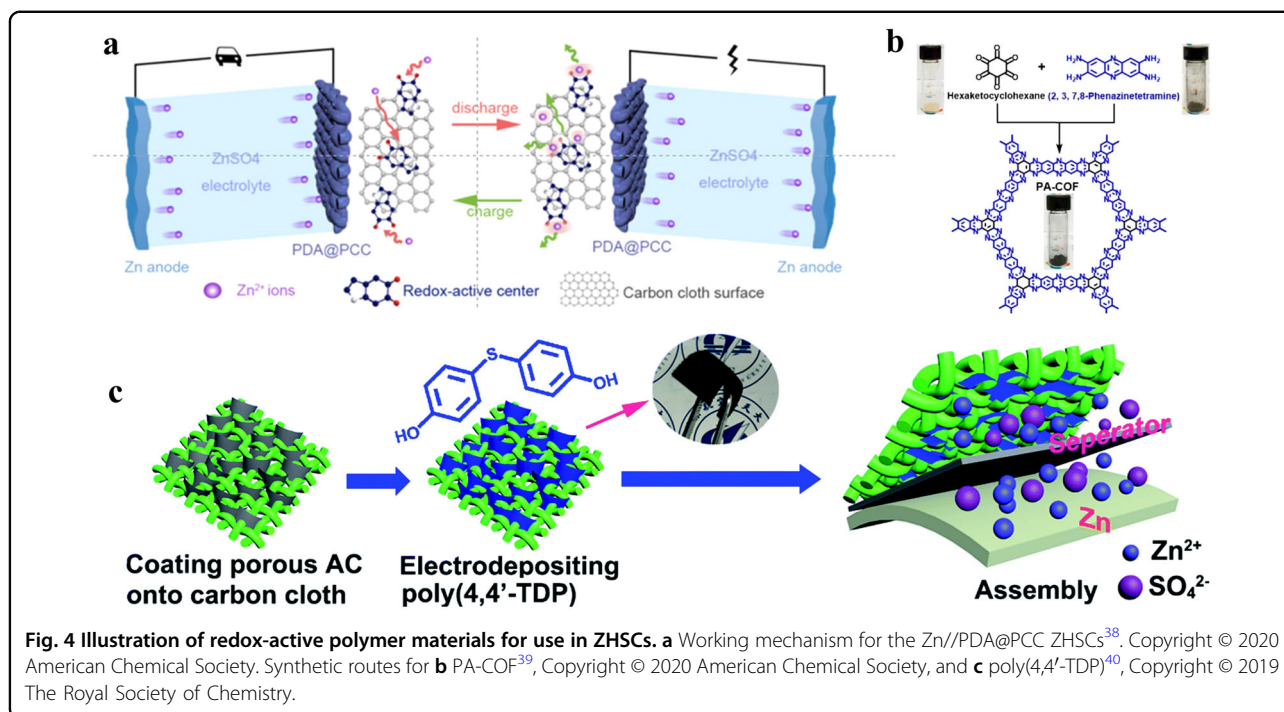
MXenes and improving the stability of the structure by embedding other substances between the layers are effective ways to extend the lifetimes of ZHSCs.

### Redox-active polymers

Cost-effective, safe, and environmentally friendly, redox-active polymers with fast and reversible redox reactions are promising materials for various energy storage devices. Polydopamine (PDA) has several redox-active sites and can be used as a redox-active agent to increase the Zn-ion storage capacitance. PDA-coated carbon cloths (PDA@PCC) were fabricated as cathodes for aqueous ZHSC through air calcination and hydrothermal treatment<sup>38</sup>. The abundant oxygen-containing groups and large specific surface areas facilitated the adsorption of Zn ions. Ex situ XPS and EDS demonstrated that  $\text{Zn}^{2+}$  underwent quinone coordination reactions, electrical double-layer absorption/desorption at the cathode, and deposition/exfoliation at the anode (Fig. 4a). Inspired by the modular nature of the covalent organic framework (COF), a phenanthroline covalent organic framework (PA-COF) was developed with an electron-rich backbone and nitrogen-rich active sites for use as cathodes in ZHSCs (Fig. 4b)<sup>39</sup>. The  $\text{Zn}^{2+}/\text{H}^+$  coininsertion mechanism was confirmed with electrochemical analyses and solid-state NMR, and the phenanthroline functional group was demonstrated to be the active site for Zn-ion storage. The capacitance decay of the assembled ZHSCs was only 0.38% after more than 10,000 cycles. Poly(4,4'-thiodiphenol, TDP)-modified nanoporous AC was used with Zn foil to assemble the ZHSCs (Fig. 4c), and the redox-active carbonyl groups responsible for charge storage in the poly(4,4'-TDP) molecular chains increased the capacitance and expanded the voltage window (0.1–1.9 V)<sup>40</sup>.

### Other cathode materials

In addition to the cathode materials discussed above, there are several other emerging cathodes for ZHSCs, such as siloxanes, phosphorene, and TiN. Although silicon is nontoxic and abundant, there have been few reports on the use of silicon-based materials as electrodes for ZHSCs. In 2021, the use of few-layered siloxanes as cathodes for ZHSCs was reported for the first time<sup>41</sup>. Theoretical calculations suggested that the Zn ions preferred to be adsorbed on the Si–Si rings of the siloxene. The diffusion energies for Zn ions on monolayer or tri-layer siloxenes were calculated to be much lower than that for the bulk silicon suboxide. The assembled ZHSCs based on few-layer siloxanes exhibited excellent rate performance (71.4% at 5  $\text{mA cm}^{-2}$ ) and excellent capacitance retention (94.3%) after 16,000 cycles. Like few-layer siloxanes, few-layer phosphorene (FL-P) has a large specific surface area, abundant adsorption sites, good



mechanical strength, and high carrier mobility and thus is a potential material for supercapacitors. Recently, electrochemical exfoliation was applied to obtain 2D FL-P cathodes<sup>42</sup>. The operating voltages of the assembled ZHSCs with high salt concentrations were increased to 2.2 V, and a capacitance of 145.9 F g<sup>-1</sup> was maintained even at 6.4 A g<sup>-1</sup>. When Et<sub>4</sub>NBF<sub>4</sub>/PC was used as the electrolyte, the voltage increased to 2.5 V. TiN was creatively proposed as a cathode for ZHSCs, and its electrochemical properties in different electrolytes were compared<sup>43</sup>. Studies based on the energy difference and adsorption sites of SO<sub>4</sub><sup>2-</sup>, Ac<sup>-</sup> and Cl<sup>-</sup> on TiN materials demonstrated that the SO<sub>4</sub><sup>2-</sup> anion had the lowest adsorption energy and the best electrochemical properties.

## Functional anode materials

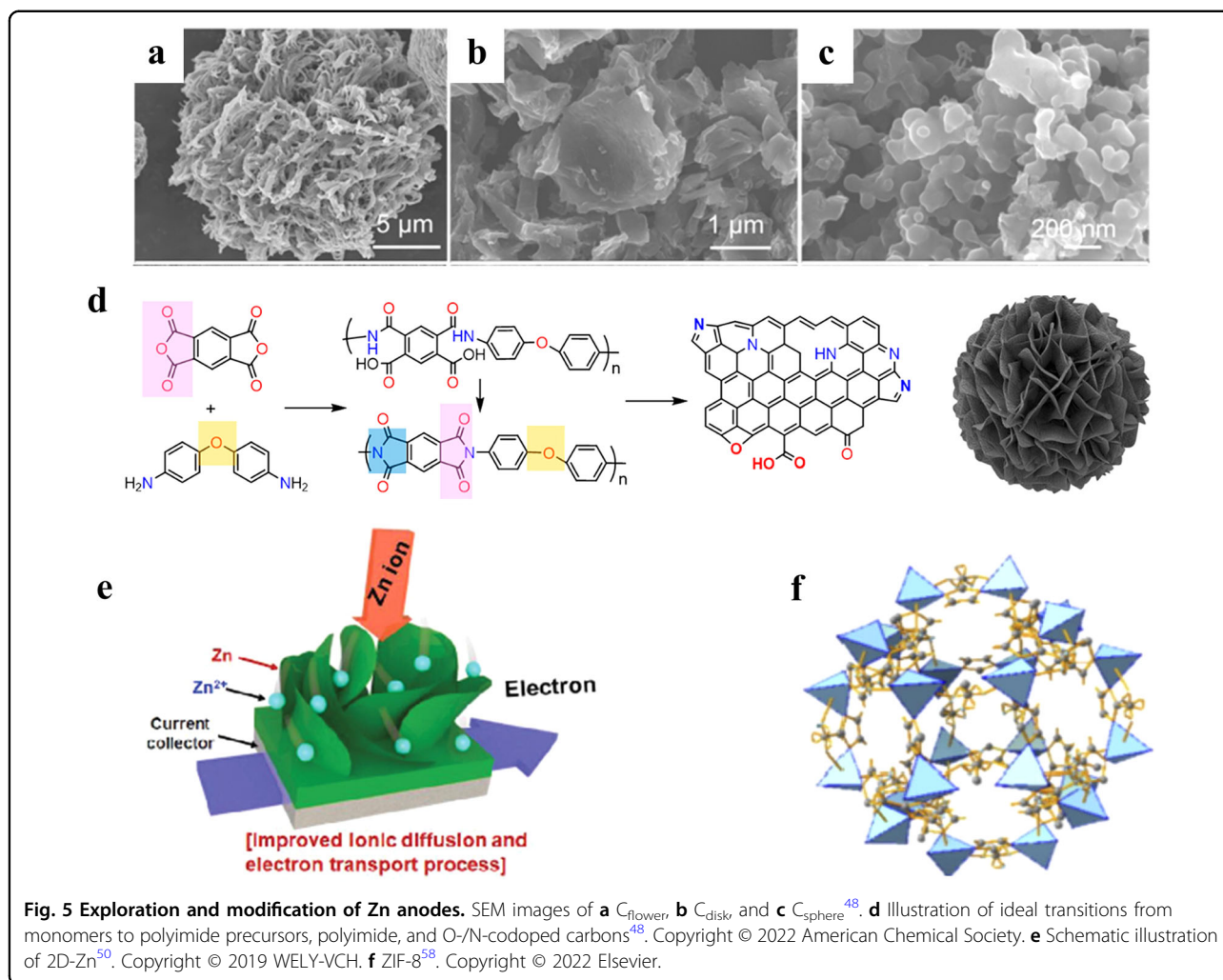
### 3D Zn composites

With a high theoretical specific capacity and a low redox potential, Zn is one of the most promising anode materials for aqueous energy storage systems<sup>44</sup>. When Zn is used as an anode material for ZHSCs, problems such as dendrite growth, corrosion, and hydrogen evolution often occur. Moreover, excessive use of the Zn in ZHSCs can lead to a waste of resources. To solve these problems, various strategies, such as optimizing the Zn structure, alloying, and modifying the coating surface, have been proposed.

3D Zn structures or porous Zn sponges inhibited the growth of Zn dendrites on surfaces in contact with the

septum and limited dendrite formation within the internal porous structure<sup>45–47</sup>. Different carbon substrates for Zn anodes were designed and constructed by controlled self-assembly of the corresponding polymer precursors<sup>48</sup>. A comparison of carbon flowers (C<sub>flower</sub>), carbon disks (C<sub>disk</sub>), and carbon spheres (C<sub>sphere</sub>) revealed that C<sub>flower</sub>, composed of outwardly oriented nanoribbons, had a 3D nanostructure with abundant pores and zincophilic oxygen/nitrogen doping (Fig. 5a–d). Among them, ether, carboxyl, and pyrrole nitrogen groups guided nucleation and growth of the Zn in a heterogeneous epitaxial mode. As a result, the assembled ZHSCs exhibited longer lifetimes without dendrite overgrowth.

With an electrodeposition strategy, a Zn anode with a large specific surface area was obtained, which prevented the formation of Zn dendrites. Zeolite imidazole framework-8 (ZIF-8), a traditional MOF, was synthesized, and the Zn<sup>2+</sup> in the framework was thermally reduced to form a trace amount of ZnO after heat treatment at 500 °C. The thus-prepared Zn@ZIF-8-500 was used as the anode for a ZHSC<sup>49</sup>. The inherent porous structure and trace amounts of ZnO in the framework increased the number of nucleation sites, provided uniform deposition, and blocked side reactions. The assembled Zn@ZIF-8-500//AC supercapacitors exhibited excellent stabilities and retained 72% of the capacitance and 100% of the coulombic efficiency after 20,000 cycles. In addition, a 2D layered nanostructured Zn (2D-Zn) anode was constructed by electroplating (Fig. 5e)<sup>50</sup>. Due to the 2D structure, the ion diffusion rate increased, and the

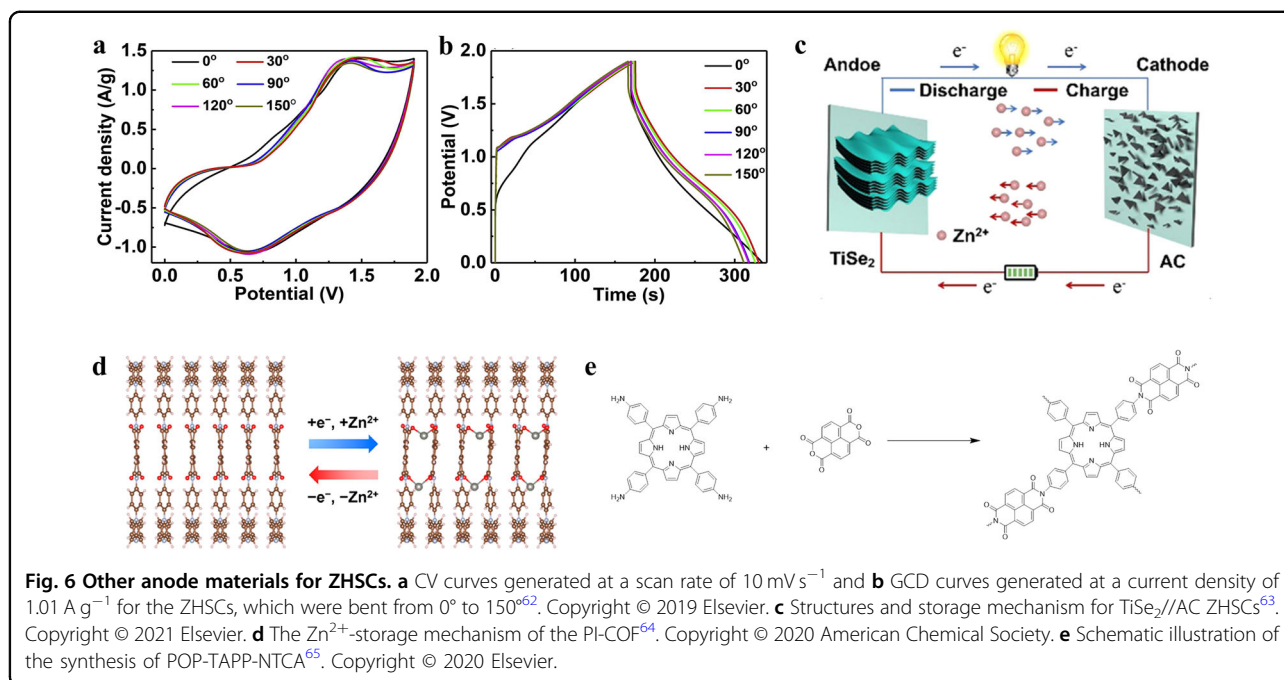


assembled supercapacitor had a high energy density and a long cycling life.

Alloying provided Zn deposition sites induced uniform deposition and stripping of Zn. A deep eutectic solvent (DES) was developed for Cu–Zn alloying reactions, which produced a Cu–Zn alloy with a Zn-rich interlayer. The resulting alloy had a high Zn utilization ratio with uniform Zn plating/stripping reactions<sup>51</sup>. DES-Zn//AC capacitors showed 70.9% capacitance retention after 7000 cycles at a current density of  $4 \text{ A g}^{-1}$ . Alternatively, due to the low melting point of Hg, zinc amalgams ( $\text{Zn}_3\text{Hg}$ ) can be synthesized at room temperature<sup>52</sup>. Instantaneous alloying of the formed  $\text{Zn}_3\text{Hg}$  prevented dendrite growth and corrosion. Thus, the  $\text{Zn}_3\text{Hg}$  anode exhibited a cycling life of 2000 h. Moreover, compared with Zn//AC ( $64 \text{ mAh g}^{-1}$ ,  $0.1 \text{ A g}^{-1}$  and 1827 h,  $2 \text{ A g}^{-1}$ ),  $\text{Zn}_3\text{Hg}$ //AC exhibited a higher capacity ( $80 \text{ mAh g}^{-1}$ ,  $0.1 \text{ A g}^{-1}$ ) and longer lifetime (5000 h,  $2 \text{ A g}^{-1}$ ).

Protecting Zn anodes by modifying the functional interphase layers has been effective in reducing

polarization, inhibiting dendrite formation, and enhancing interfacial stability<sup>53–57</sup>. Mesoporous hollow carbon sphere interlayers on Zn foils were used to regulate dendrite/protrusion growth on Zn anodes<sup>16</sup>. Moreover, MOFs are interesting coating and modification interlayers for Zn anodes due to their large surface areas and adjustable pore sizes. A simpler approach was taken to synthesize ZIF-8 (Fig. 5f)<sup>58</sup>. ZIF-8, which grew in situ on the surface of Zn, is hydrophobic and enables homogeneous deposition of Zn during charge–discharge processes and inhibits side reactions. Thus, the prepared dendrite-free Zn electrodes exhibited low polarization ( $89.0 \text{ mV}$  at  $10 \text{ mA cm}^{-2}$ ) and high cycling stabilities (more than 800 h at  $10 \text{ mA cm}^{-2}$ ), and the developed ZHSC exhibited a high capacitance retention rate of 96% after 13,000 cycles at  $5 \text{ A g}^{-1}$ . Konjac glucomannan (KGM) is composed mainly of  $\beta$ -d-glucose and  $\beta$ -d-mannose. The numerous oxygen functional groups served as active sites to redistribute the  $\text{Zn}^{2+}$  concentration field. Therefore, Zn anodes with KGM coatings ( $\text{Zn@KGM}$ )



were carefully designed<sup>59</sup>. Due to the strong coordination ability triggered by the  $-\text{OH}$  and  $=\text{CO}$  groups,  $\text{Zn}^{2+}$  flux was coordinated, and the tip effect was suppressed.  $\text{Zn@KGM//AC}$  exhibited a capacitance retention rate of 98.8% after 5000 cycles. Our group also investigated the effects of different interlayers on the modification of Zn anodes. By comparing the electrochemical performance and deposition principles of Zn anodes modified with pure electronic, ionic, and hybrid conductor coatings, the hybrid coating-modified Zn anodes ( $\text{Alg-Zn+AB@Zn}$ ) combined the advantages of both electronic and ionic conductors and exhibited longer cycle lives. The assembled  $\text{Alg-Zn+AB@Zn//AC}$  exhibited an excellent cycling life of up to 16,000 cycles<sup>60</sup>.

### Zn-free anodes

Typically, excess Zn is used as the anodes in ZHSCs, which leads to a low energy density for the whole device. Moreover, the electrochemical properties of ZHSCs with excessive Zn anodes were not reliable enough for practical application<sup>61</sup>. Therefore, further research into new anode materials with lower redox potentials than Zn for ZHSCs is needed to enable commercial applications of ZHSCs. Here, zinc-free anodes refer to Zn host materials without Zn. AC is a typical Zn-free anode and was an early alternative to the Zn anodes in ZHSCs<sup>25,28</sup>. However, when AC was used as a capacitive electrode, it exhibited limited capacitance due to the energy storage mechanism of the electrochemical double-layer capacitor.

Due to their high electrical conductivities, hydrophilic surface areas, and pseudocapacitive mechanisms, MXenes

are potential research objects. New ZHSCs were fabricated with a binder-free MXene ( $\text{Ti}_3\text{C}_2\text{T}_x$ ) anode. The absence of binders and conductive additives reduced the weight of the electrodes and increased the energy density of the ZHSC device<sup>26</sup>. Therefore, a high energy density ( $98.6 \text{ Wh kg}^{-1}$ ) and high power density ( $2481 \text{ W kg}^{-1}$ ) were achieved. Moreover, cotton cloth was placed in a solution containing MXene ( $\text{Ti}_3\text{C}_2\text{T}_x$ ) to obtain MXene@COC with different MXene mass loadings, which were subsequently used as anodes for ZHSCs<sup>62</sup>. The assembled ZHSCs exhibited excellent electrochemical properties, such as high energy densities ( $90 \text{ Wh kg}^{-1}$ ) and high power densities ( $3838 \text{ W kg}^{-1}$ ). They also showed excellent flexibility. Even if the temperature was increased to  $150^\circ$ , the CV and GCD curves basically remained unchanged (Fig. 6a, b). Similarly,  $\text{Ti}_3\text{C}_2\text{T}_x$  MXene anodes were fabricated by electrodeposition on graphite paper substrates, and the assembled ZHSCs exhibited good electrochemical stabilities, maintained 77% of the initial capacitance, and showed  $\sim 98\%$  coulombic efficiency after 10,000 cycles<sup>29</sup>.

In addition,  $\text{TiSe}_2$  was used in a Zn-ion energy storage system for the first time, and the feasibility of using  $\text{TiSe}_2$  for (de)intercalation of Zn ions was demonstrated through experiments and theoretical calculations (Fig. 6c)<sup>63</sup>. The  $\text{TiSe}_2$  electrode works over a low voltage range of  $0.05\text{--}0.60 \text{ V}$  vs.  $\text{Zn/Zn}^{2+}$ . Over a wider voltage range of  $0.05$  to  $1.80 \text{ V}$ , the fabricated ZHSC with the  $\text{TiSe}_2$  anode and activated carbon (AC) cathode exhibited a specific capacitance of  $60.6 \text{ F g}^{-1}$  at  $0.20 \text{ A g}^{-1}$ . The  $\text{Zn}^{2+}$  diffusion coefficient in the  $\text{TiSe}_2$  anode was calculated to be in

the range of  $10^{-9}$ – $10^{-10}$   $\text{cm}^2 \text{s}^{-1}$ , which was greater than those of many metal oxide electrodes.

Most organic materials reported for  $\text{Zn}^{2+}$  storage have high redox potentials ( $>1$  V vs.  $\text{Zn}^{2+}/\text{Zn}$ ), making them more suitable for use as cathodes than anodes. However, a 2D polyarylimide covalent organic framework (PI-COF) anode with rapid  $\text{Zn}^{2+}$  storage kinetics was designed<sup>64</sup>. The sloped charge/discharge curves of the PI-COF electrode without a clear voltage plateau indicated charge storage behavior similar to that of a supercapacitor. Additionally, PI-COF electrodes stored  $\text{Zn}^{2+}$  through a two-step redox process, which involved enolate formation through progressive coordination of carbonyl oxygens with  $\text{Zn}^{2+}$  in a reversible manner (Fig. 6d). In addition, our group<sup>65</sup> constructed a polymeric tetra(4-aminophenyl)porphyrin-1,4,5,8-naphthalenetetracarboxylic dianhydride (POP-TAPP-NTCA) from PI and porphyrin, and it served as a Zn storage anode formed via a scalable bottom-up strategy (Fig. 6e). The storage of Zn ions in microspherical POP-TAPP-NTCA involved both Faradaic and non-Faradaic processes. Density functional theory (DFT) calculations revealed that the carbonyl and porphyrin nitrogen sites of POP-TAPP-NTCA enabled the storage of Zn ions, but storage of the Zn ions at the porphyrin nitrogen sites was irreversible.

For Zn-free anode hybrid supercapacitors, the problem is poor stability ( $<85\%$ ). Therefore, in the future, it is necessary to explore new anode and cathode materials and optimize the electrolyte for Zn-free anode hybrid supercapacitors.

## Functional electrolyte materials

### Organic/ionic liquid electrolytes

The widely used aqueous electrolytes in ZHSCs have narrow electrochemical stability windows. To increase the operating voltages of ZHSCs, researchers have developed a series of organic and ionic liquid electrolytes.

Recently, an ionic liquid (IL) electrolyte was used to increase the voltage to 2.4 V, thus greatly increasing the volumetric energy density to 4.3  $\text{Wh L}^{-1}$ <sup>66</sup>. Furthermore, after the ILs were replaced with acetonitrile (AN) and  $\text{ZnCF}_3\text{SO}_3$ , the power density of the ZHSC increased from 17.7  $\text{kW L}^{-1}$  to 18.8  $\text{kW L}^{-1}$ , and no capacitance degradation was observed after 60,000 cycles. Then, a new hybrid electrolyte ( $\text{Zn}(\text{TFSI})_2/[\text{Pyr}_{14}\text{TFSI}]_{16}/[\text{AN}]_4$ ) was designed by combining a Zn salt ( $\text{Zn}(\text{TFSI})_2$ ), an organic solvent (AN), and an IL ( $\text{Pyr}_{14}\text{TFSI}$ )<sup>67</sup>. Due to the synergistic effect of  $\text{Pyr}_{14}\text{TFSI}$  and AN, the electrochemical window was widened to 3.3 V vs.  $\text{Zn}/\text{Zn}^{2+}$ . As a result, the ZHSCs had high operating voltages (2.1 V) and very good cycling stabilities. In addition to increasing the voltage window, the ionic electrolytes (such as  $\text{Zn}(\text{BF}_4)_2/[\text{EMIM}]\text{BF}_4$ ) optimized the deposition of the Zn anode<sup>68</sup>. Due to the high reduction/oxidation stability of  $\text{Zn}(\text{BF}_4)_2/$

$[\text{EMIM}]\text{BF}_4$ , the formation of Zn dendrites and the occurrence of side reactions during the charging and discharging processes were avoided. Therefore, after cycling for 1200 h, the coulombic efficiency was still as high as 99%. Similarly, a ZHSC was fabricated with organic N,N-dimethylformamide (DMF) containing  $\text{Zn}(\text{TFSI})_2$ , which, owing to the presence of  $\text{Zn}^{2+}$ -DMF complexes, allowed uniform deposition of Zn ions while avoiding irreversible hydrogen evolution reactions<sup>69</sup>. Impressively, the assembled hybrid supercapacitor worked between  $-65$  °C and  $100$  °C because of its low freezing point and high boiling point.

### Water in salt electrolytes

The water in salt electrolytes (WiSs) provides extended potential windows, suppression of water splitting reactions, and improved safety and thus shows potential for use in ZHSCs.

ZHSCs with aqueous  $\text{ZnCl}_2$  electrolytes exhibited superior capacitances and rates compared to ZHSCs with aqueous  $\text{ZnSO}_4$ ,  $\text{Zn}(\text{CF}_3\text{SO}_3)_2$ ,  $\text{Zn}(\text{Ac})_2$  and  $\text{Zn}(\text{NO}_3)_2$  electrolytes<sup>70</sup>. Interestingly, with increasing concentrations, chloride ions ( $\text{Cl}^-$ ) caused the formation of  $[\text{ZnCl}]^+(\text{H}_2\text{O})_{n-1}$  ( $n=1-6$ ). The solvation and desolvation energies of  $[\text{ZnCl}]^+(\text{H}_2\text{O})_{n-1}$  ( $n=1-6$ ) were significantly lower than those of  $[\text{Zn}(\text{H}_2\text{O})_n]^{2+}$ , which favored desolvation. Accordingly, a salt-in-water hydrogel electrolyte filled with  $\text{ZnCl}_2$  was constructed for use in ZHSCs. In contrast, the effects of different aqueous  $\text{ZnCl}_2$  concentrations on the adsorption/desorption of Zn on MXene electrodes were explored<sup>71</sup>. It is clear that the electrode performance was improved due to the acidity of the electrolyte at high concentrations, leading to both Faradaic (redox by proton insertion) and non-Faradaic (proton and  $\text{Zn}^{2+}$  adsorption) reactions at the MXene electrodes. Generally,  $\text{ZnCl}_2$  is the most common salt for high-voltage ZHSCs in WiSs. In addition, acetates are also used in WiSs. The effects of different potassium acetate (KAc) and zinc acetate ( $\text{ZnAc}_2$ ) ratios on Zn plating/stripping were systematically examined<sup>72</sup>. The 30 m KAc + 1 m  $\text{ZnAc}_2$  electrolyte showed the highest reversibility and stability for Zn plating/stripping ( $m = \text{mol kg}^{-1}$ ). The coulombic efficiency of the assembled ZHSCs approached 100% after 10,000 cycles.

### Redox electrolytes

Great effort has been expended to optimize electrolytes and increase the energy densities and cycling stabilities of ZHSCs. The introduction of redox additives into the electrolyte usually induces additional redox reactions (additional redox couples into the electrolyte) on the electrode surfaces, through which the capacitance and energy density of the ZHSC are significantly increased.

Inspired by Zn-iodine batteries, ZHSCs were designed and fabricated with B,N dual-doped porous carbon

microtubes (BN-CMT) and Zn as the cathode and anode, respectively, and the ultrahigh capacity ( $416.6 \text{ mAh g}^{-1}$ ) and energy density ( $472.6 \text{ Wh kg}^{-1}$ ) were increased by introducing redox-active iodide ions into the electrolyte<sup>73</sup>. The capacity retention rate of the ZHSC was 99.1% after 10,000 cycles. Additionally, based on the above research, a hydrogel electrolyte was designed with  $\text{ZnBr}_2$ <sup>74</sup>. Owing to the additional Faradaic contribution provided by the redox reaction ( $3\text{Br}^-/\text{Br}_3^-$ ) occurring at the electrode/electrolyte interface, a high energy density of  $605 \text{ Wh kg}^{-1}$  was maintained at a power density of  $1848 \text{ Wh kg}^{-1}$ . In addition, a Zn-bromine “supercapattery” system consisting of an S/P codoped carbon-based cathode, a carbon cloth (CC) anode, and an electrolyte with a soluble double redox additive ( $3\text{Br}^-/\text{Br}_3^-$ ) was constructed<sup>75</sup>. The anode exhibited electrochemical double-layer capacitive charge storage from the CC, pseudocapacitive charge storage from the underpotential deposition of monolayer  $\text{Zn}^{2+}$  on the surface of the CC, and battery-type  $\text{Zn}^{2+}$  deposition on the Zn//CC surface. Similarly, the charge storage contributions of the S/P codoped carbon cathodes resulted from capacitive/pseudocapacitive processes below potentials of  $1.3 \text{ V vs. Zn/Zn}^{2+}$  and from battery-type processes in the voltage range  $1.3 - 1.8 \text{ V vs. Zn/Zn}^{2+}$ . Hence, after integrating the triple functions of capacitive/pseudocapacitive and battery-type charge storage in both the cathode and anode, the assembled ZHSC achieved a battery-level energy density and a capacitor-level power density.

### Polymer electrolytes

To address the inevitable leakage of liquid electrolytes from flexible ZHSCs, there is a strong need to develop electrolytes that combine high ionic conductivity, good mechanical and electrochemical stability, excellent wettability, and a high safety profile. Through rational design, polymer or quasisolid electrolytes may be useful candidates. Polymeric or quasisolid electrolytes consist mainly of Zn salts, polymeric backbones, and small amounts of water. Common polymeric backbones include PVA<sup>76,77</sup>, PAA<sup>78</sup>, PAM<sup>36,79</sup>, gelatin<sup>80,81</sup>, etc. For example, polymer electrolytes were used in ZHSCs by adding copolymer-derived hollow carbon spheres, Zn deposited on carbon cloth, and a polyacrylamide hydrogel as the cathode, anode, and electrolyte, respectively<sup>79</sup>. The assembled ZHSCs exhibited excellent cycling stability (98% capacitance retention after 15,000 cycles at a current density of  $1 \text{ A g}^{-1}$ ). In addition, supramolecular gel polymer electrolytes (SGPEs) formed dynamic reversible physical cross-linking with hydrogen bonds, ionic bonds and  $\pi$ - $\pi$  interactions exhibiting the advantages of simple fabrication methods and environmental friendliness<sup>82</sup>. The assembled Zn@SGPE//AC exhibited a long cycling life with 84% capacity retention after 110,000 cycles at  $5 \text{ A g}^{-1}$ .

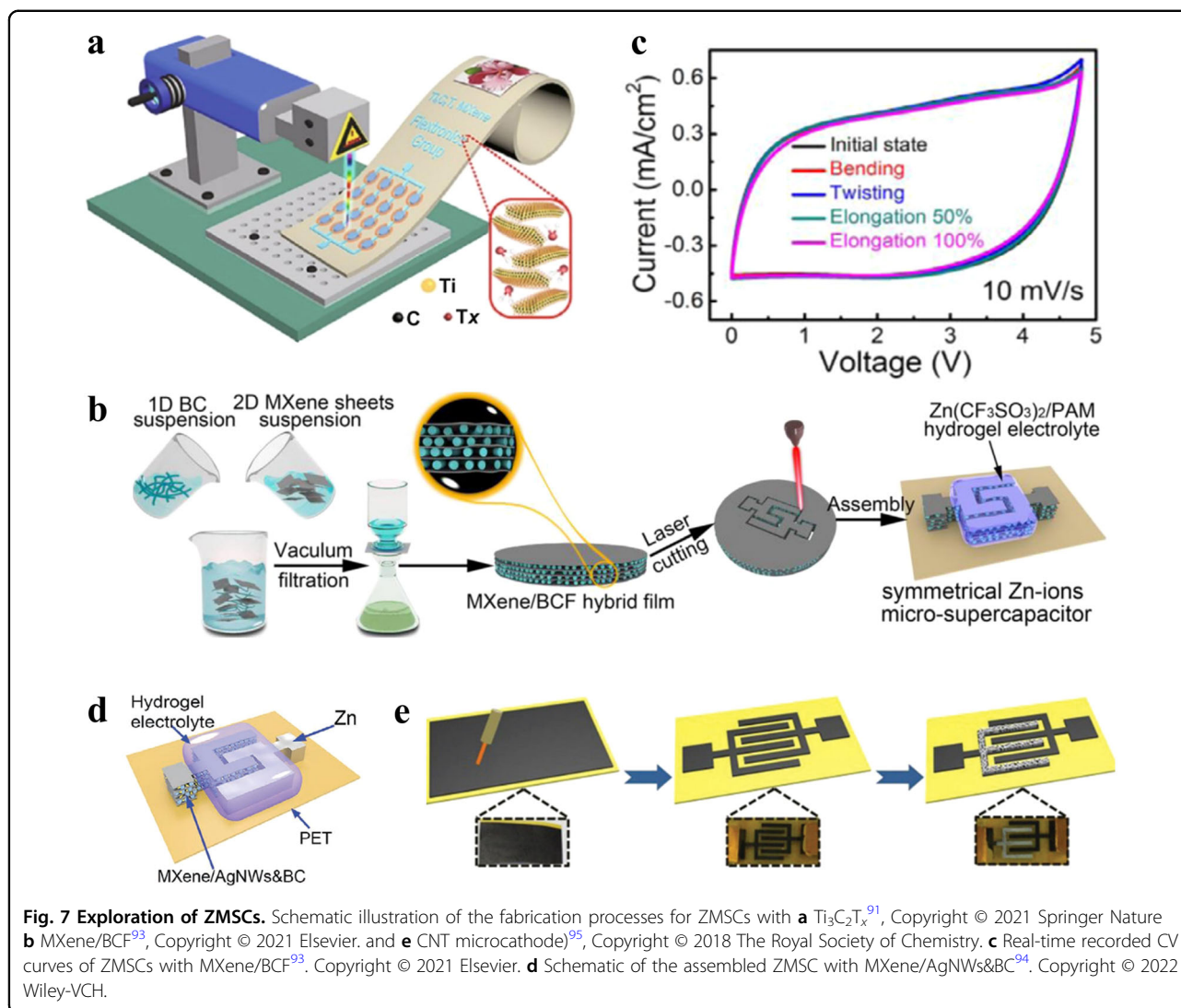
To meet the operating requirements of ZHSCs, composite polymers or quasisolid electrolytes that combine the advantages of individual components have been explored extensively. For example, electrolytes consisting of sodium alginate (SA)/polymethacrylic combinations displayed excellent regeneration capabilities<sup>83</sup>. In addition, a frost-resistant hydrogel electrolyte (AF-PVC-CMC/Zn( $\text{CF}_3\text{SO}_2$ )) was prepared by adding ethylene glycol (EG) to a network of antifreeze polyvinyl alcohol carboxymethyl cellulose (AF-PVA-CMC) containing aqueous  $\text{Zn}(\text{CF}_3\text{SO}_3)_2$ <sup>84</sup>. An AF-PVA-CMC/Zn( $\text{CF}_3\text{SO}_2$ ) electrolyte with enhanced mechanical properties enabled uniform Zn deposition and hindered dendrite overgrowth. Additionally, due to the high boiling point and high dielectric constant of ethylene glycol (EG), the interaction between polyvinyl alcohol and ethylene glycol inhibited the formation of ice crystals and prevented freezing at low temperatures. Therefore, EG is often used as an antifreeze in ZHSCs<sup>85,86</sup>. In general, gel electrolytes tend to fail at high temperatures. As a response, heat-resistant and nonflammable polymer electrolyte (HRNPE) films with the pyrrolidinium-based IL (1-methyl-1-propylpyrrolidine bis(trifluoromethyl sulfonyl)imide) as an additive were prepared<sup>87</sup>. ZHSCs with HRNPE separators had safe operating temperatures of up to  $100^\circ\text{C}$ . At room temperature, the developed ZHSCs showed a capacitance retention rate of 88% after 10,000 cycles and cycled 30,000 times even at a high temperature of  $80^\circ\text{C}$ .

### Functional devices

#### Miniaturized devices

Compared with traditional supercapacitors, the small sizes and footprints of Zn-ion hybrid micro-supercapacitors (ZMSCs) enable their use with multifunctional devices in nanorobots, wireless sensor networks, microelectromechanical systems, and wearable flexible electronics<sup>88</sup>. This all-in-one compact device increases work efficiency and reduces maintenance costs<sup>89-91</sup>.

ZMSCs were assembled with AC and electroplated with Zn<sup>92</sup>. The as-prepared ZMSCs exhibited large areal capacitances ( $1297 \text{ mF cm}^{-2}$  at  $0.16 \text{ mA cm}^{-2}$ ) and high energy densities ( $115.4 \text{ } \mu\text{Wh cm}^{-2}$  at  $0.16 \text{ mW cm}^{-2}$ ). Subsequently, a simpler laser writing method was proposed to construct a ZMSC with  $\text{Ti}_3\text{C}_2\text{T}_x$  as the cathode (Fig. 7a)<sup>91</sup>. After proper annealing, the ZMSC exhibited excellent capacitance retention (80%, 50,000 cycles) and rate stability ( $2.02 \text{ mF cm}^{-2}$ ,  $10 \text{ mV s}^{-1}$ ). Furthermore, a single ZMSC drove a digital timer even when the ZMSC was bent. As shown in Fig. 7b, a ZMSC with a wide voltage window ( $1.2 \text{ V}$ ) based on MXene/bacterial cellulose fibers (BCFs) and Zn and  $\text{Zn}(\text{CF}_3\text{SO}_3)_2/\text{PAM}$  hydrogel electrolytes was manufactured<sup>93</sup>. The areal energy densities of the ZMSCs were significantly increased to

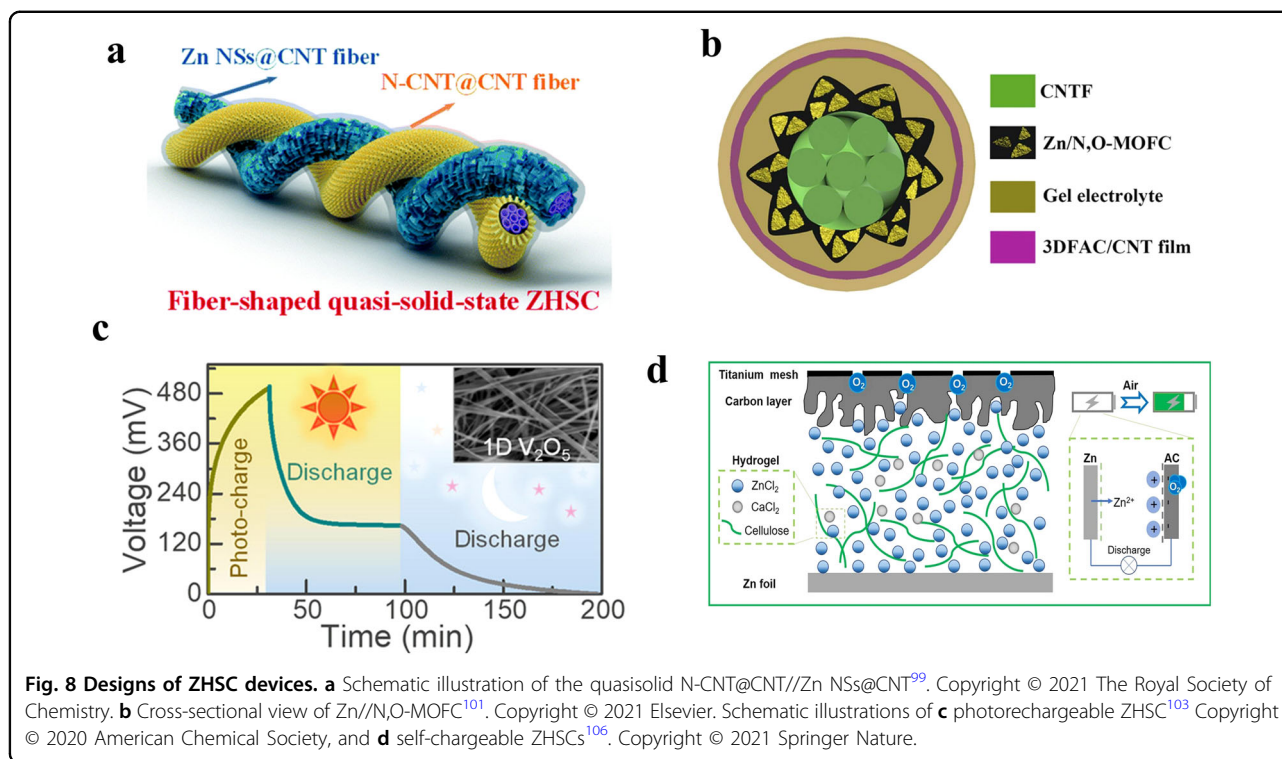


$34.0 \mu\text{Wh cm}^{-2}$ , in part due to the suppressed hydrogen/oxygen evolution reactions within the MXene/BCF main electrode. A stretchable ZMSC array (ZMSCA) consisting of a screen-printed liquid metal bridge (LMBI) and ZMSCs was constructed, and it exhibited considerable variability and stable electrochemical properties. The CV curves recorded in real-time did not change significantly even when the sample was stretched by 100%, bent  $180^\circ$ , or twisted  $360^\circ$ , and the curves maintained the same shape as the original curves (Fig. 7c). In addition, ZMSCs that combine ionic intercalation and solid-solid redox reactions have been described<sup>94</sup>. The ZMSCs were composed of MXene/Ag nanowires (AgNWs), a bacterial cellulose (BC) cathode, a Zn anode and a PAM/ $\text{ZnCl}_2 + \text{NH}_4\text{Cl}$  hydrogel electrolyte (as shown in Fig. 7d). The presence of AgNWs in MXene/AgNWs&BC extended the interlayer space and enhanced ion intercalation and reversibility while providing an additional phase transition ( $\text{Ag} + \text{Cl}^-$

$\rightleftharpoons \text{AgCl}$ ) to create a flat discharge plateau, which increased the charge storage capacitance and output stability. Therefore, energy densities of up to  $227 \mu\text{Wh cm}^{-2}$  were achieved. Notably, ZMSCs can also be fabricated via laser engraving and electroplating techniques. Figure 7e shows the preparation processes of ZMSCs with Zn microanodes and CNT microcathodes<sup>95</sup>. The energy densities of the as-prepared ZMSCs reached  $29.6 \mu\text{Wh cm}^{-2}$ . More importantly, an in situ Zn-supplemented electroplating method was developed. This method avoided irreversible consumption of the Zn anode and decreased the capacitance and cycling life without destroying the ZMSCs.

#### Fiber-shaped devices

The development of portable, bendable, foldable, and wearable energy storage devices is crucial for flexible electronic devices, such as smart textiles, robots, and



biosensors<sup>96,97</sup>. As emerging energy storage devices, Zn-ion fiber hybrid supercapacitors (ZFSCs) are gradually attracting the attention of researchers due to their attractive features, such as long cycling lives, low costs, safety, and environmental friendliness<sup>80,98</sup>.

The first ZFSC was fabricated with rGO/CNTs, Zn-coated graphite fibers, and a polyacrylic acid (PAA) hydrogel containing ZnSO<sub>4</sub> as the cathode, anode and quasisolid electrolyte, respectively<sup>78</sup>. Impressively, the assembled ZFSCs exhibited 98% capacitance retention after 10,000 charge/discharge cycles, demonstrating a long cycling life and excellent stability. The ZFSCs showed excellent mechanical flexibilities as a result of the PAA hydrogel electrolytes and fiber-shaped electrodes. Researchers subsequently explored ZFSCs, particularly for use as cathode materials. Because of the fast electron transport kinetics and high specific surface areas, a 3D N-doped carbon nanotube architecture@carbon nanotube (N-CNT@CNT) was constructed for use in ZFSCs (Fig. 8a)<sup>99</sup>. The operating voltages of the assembled quasisolid ZFSCs were extended to 1.8 V. At different scan rates, all CV curves exhibited nearly rectangular shapes with fast current responses, demonstrating typical capacitive behavior, excellent reversibility, and ultrafast charge/discharge capability. Moreover, the Zn storage performance of onion-like carbon (OLC) was enhanced by the introduction of nitrogen and phosphorus<sup>100</sup>. The structural stability of the OLC and the synergistic effect of N and P endowed the assembled aqueous supercapacitor with

excellent electrochemical stability (77.8% capacitance retention after 50,000 cycles at 10 mA cm<sup>-2</sup>). Furthermore, compared with the carbon cathodes formed by coating, the N, P-OLC@ carbon cloth (N, P-OLC@CC), which was formed via in situ deposition of the OLC on CC and annealing, exhibited tight bonding with the substrate. Therefore, the risk of N, P-OLC loss during bending was avoided. The ZFSCs assembled in combination with Zn anodes exhibited high energy densities (32.1 mWh cm<sup>-2</sup>) and high power densities (48.3 W cm<sup>-2</sup>). Moreover, after wrapping the AC@CF with cellulose paper, 2D-Zn@CF was wound on the cellulose paper<sup>50</sup>. Thus, the fabricated ZFSCs in a 1 M ZnSO<sub>4</sub>/PVA gel electrolyte exhibited excellent electrochemical performance (25 μWh cm<sup>-2</sup>, 50 μW cm<sup>-2</sup>) and high mechanical flexibility. Moreover, good working conditions were maintained even under water.

The morphologies and electrochemical activities of Zn anodes have also restricted the practical application of ZFSCs. As a solution to this challenge, highly reversible fibrous Zn anodes with controlled deposition morphologies were developed by electroplating and depositing Zn nanosheets on a carbon-derived 3D MOF containing N and OH functional groups (N,O-MOFCs) (Fig. 8b)<sup>101</sup>. Due to the layered structure and fast ion diffusion, the specific volumetric capacitances of the ZFSCs reached 128.06 F cm<sup>-3</sup>, and the volume energy density was as high as 57.63 mWh cm<sup>-3</sup>. More importantly, the highly efficient rechargeability of the fibrous Zn anode also ensured

that the ZFSC device was sufficiently stable, with a capacitance retention rate of 99.20% after 10,000 charge-discharge cycles.

### Self-chargeable devices

Energy can be directly obtained from the surrounding environment by integrating energy conversion technology and energy storage units into all-in-one energy storage devices. Solar energy is a common source of energy and is now widely used in energy conversion devices. Graphitic carbon nitride electrodes serve as both capacitive electrodes and light-harvesting materials with the help of a conductive additive allowing electrons to pass through an external circuit. The first photorechargeable ZHSC was proposed in 2015<sup>102</sup>. However, the photocharged energy density of this system based on graphitic carbon nitride electrodes was still unsatisfactory (only  $0.7 \text{ Wh kg}^{-1}$ ) and must be increased. An optimized scheme with vanadium oxide nanofibers used as optically and electrochemically active electrodes and silver nanowires as conductive additives in a photorechargeable ZHSC was subsequently proposed by the same research group (Fig. 8c)<sup>103</sup>. Compared to carbon-based conductive additives, silver nanowires supported photoexcited hole transport and provided light scattering centers that enhanced visible light absorption. In comparison with that of the previous system, the photocharge energy density was increased to  $\sim 4.8 \text{ Wh kg}^{-1}$ .

Although solar energy is an easily accessible source of energy, the problem of intermittency still exists. As opposed to solar energy, air is more readily available and, therefore, more reliable. An 'air-charged' ZHSC was designed based on a U-shaped electrode, two electrolytes (a PAM hydrogel containing 2 M  $\text{ZnSO}_4$  and a sodium polyacrylate hydrogel containing 6 M KOH + 0.2 M  $\text{Zn}(\text{CH}_3\text{COO})_2$ ) and a Zn anode<sup>104</sup>. The "U-shaped" electrode in contact with the PAM was used as a capacitor electrode, and the other part was used as an air electrode. By simply peeling off the tape and allowing contact with air, the capacitor was charged to 88% in 10 min. Unfortunately, the use of an alkaline electrolyte inevitably corroded the Zn. Therefore, a new energy storage device was designed and constructed by combining a Zn-ion supercapacitor and a Zn-air battery in a mild electrolyte<sup>105</sup>. The cathode and anode of this new hybrid energy storage device were reduced to graphene oxide and Zn, respectively. Benefiting from the interactions of Zn with the oxygen-containing functional groups on the surface of graphene, the capacity of this hybrid device was increased. Additionally, the presence of defects in the graphene provided abundant active sites for the ORR, which resulted in a significant increase in the capacitances of the assembled capacitors when exposed to air. Nevertheless, since the assembled capacitors were open systems, i.e., the

electrolyzers were used as reaction vessels, further improvements are necessary for practical application. ZHSCs were constructed with high concentrations of  $\text{ZnCl}_2$  cellulose hydrogel as the electrolytes (Fig. 8d)<sup>106</sup>. The capacitor showed sustainable self-charging capability, but the self-charging capability of the ZHSCs decreased after repeated cycling, which proved that the capacitor was not reused. Therefore, it is also necessary to restore the usability of this capacitor by charging it with an external power source.

### Self-healing devices

Owing to the flexibility and mechanical stabilities of hydrogel electrolytes, ZHSCs based on hydrogel electrolytes show excellent electrochemical performance, but there are still several problems, such as irreversible mechanical damage and failure caused by drying. The development of self-healing devices is essential for solving the above problems.

In an earlier self-healing study of ZHSCs, multiwalled carbon nanotube (MWCNT)-RGO, MWCNT-RGO-Zn, and polyvinyl alcohol (PVA)/ $\text{Zn}(\text{CF}_3\text{SO}_3)_2$  hydrogels were utilized as cathodes, anodes and electrolytes, respectively<sup>98</sup>. Due to the great flexibility and self-healing ability of the PVA/ $\text{Zn}(\text{CF}_3\text{SO}_3)_2$  hydrogel electrolyte, the capacitance retention rates for the ZHSCs after bending and self-healing were 87.8% and 70.5%, respectively. Further studies were conducted by adding borax and nanofibrous cellulose (NFC) to PVA to prepare B-PVA/NFC composite hydrogels, which exhibited excellent flexibilities, high strengths, and toughness<sup>107</sup>. Benefiting from the dynamic reversible cross-linking between  $\text{B}(\text{OH})_4$  and hydroxyl groups, the self-healing efficiency of B-PVA/NFC was as high as 98%.

Sodium alginate (SA) is also a common material used in the preparation of gels, and the addition of SA may enhance the mechanical strengths of hydrogel electrolytes. On this basis, a new ion-conducting natural polymer hydrogel (SPMA-Zn) composed of SA-poly(methacrylic acid) was constructed<sup>83</sup>. SPMA-Zn healed rapidly when the two hydrogels remained in close contact along the cutting line without external interference. More importantly, due to dynamic and reversible interactions, even after drying and grinding into a powder, the hydrogel regained its gel form after the addition of water, demonstrating a surprising self-healing ability. The ZHSCs assembled with SPMA-Zn as the electrolyte also exhibited wide electrochemical windows (0–2.2 V) and high energy densities ( $164.1 \text{ Wh kg}^{-1}$ ). Moreover, since poly[2-(methacryloyloxy)ethyl]dimethyl-(3-sulfopropyl) (PMS) has a negatively charged sulfonic acid group and a positively charged quaternary ammonium group, the charged groups interacted with water via electrostatic forces formed ion migration channels and inhibited hydrolysis. Therefore, a self-healing double network

hydrogel electrolyte (PMAZn) consisting of PMS and SA was prepared, which exhibited a high operating voltage (2.4 V) and a fast healing response<sup>108</sup>.

In addition, a new self-healing electrolyte was designed with a multifunctional Zn ionic hydrogel and Fe<sup>3+</sup> ionic cross-linked anionic copolymers containing 2-acrylamido-2-methyl-1-propanesulfonic acid Zn/zinc acrylate/ZnCl<sub>2</sub><sup>109</sup>. The ZHSCs assembled with this hydrogel electrolyte healed quickly and recovered 89.1% of their capacitance after being completely cut.

## Summary and outlook

In conclusion, significant achievements have been made in the past few years in the designs of new electrode/electrolyte materials and novel functional devices for ZHSCs. This review outlined the latest advances in ZHSCs, with a particular focus on exploration and optimization of the cathode materials (3D carbon materials, transitional metal oxides, MXenes, redox-active polymers, etc.), modification and development of the anode materials (3D Zn composites, Zn-free anodes), regulation and development of the electrolytes (organic/ionic liquid electrolytes, WiSs, redox electrolytes, polymers or solid electrolytes) and designs of novel devices. Despite these significant advances, research on ZHSCs is still in its preliminary stage, and further exploration and innovation are still needed before practical application.

## Optimization of cathode materials

Carbon materials have been extensively studied due to their capacitive properties. In this respect, optimized structures such as porous, flower-like, and hollow spheres increase the specific surface area; doped heteroatoms (e.g., P and N) increase the number of surface adsorption sites; and the addition of oxygen functional groups increases the specific capacitance. However, the effects of various factors, such as the specific surface area (pore size, porosity, structure, etc.), on the capacitance and lifetime, the interaction of heteroatoms and oxygen functional groups with Zn ions, etc., still need to be investigated. In contrast to carbon materials, several pseudocapacitive materials, such as MXenes and redox-active polymers, have exhibited good rate performance due to their high electrical conductivities but suffer from limited cycling stabilities because of chemical/structural instability. Thus, optimization strategies such as doping, coating, and embedding are needed to improve the electrochemical stabilities of pseudocapacitive materials. These strategies also work with metal oxide cathode materials that undergo structural collapse and dissolution.

## Development of anode materials

The anode is affected by Zn dendrites, hydrogen evolution reactions, and byproduct generation, which lead to

a limited cycle life. The design of 3D Zn anodes may improve the contact with the electrolyte to reduce the formation of dendrites. Optimization of the interfacial contact between the Zn anode surface and the electrolyte would reduce the occurrence of side reactions. However, current studies do not indicate whether the 3D framework networks still have the ability to induce homogeneous Zn deposition or whether the coating would maintain interfacial stability as cycling progresses. Moreover, when coupled with cathodes, the utilization efficiencies of Zn anodes are still low, which reduces the overall energy densities of the ZHSCs. Furthermore, since the use of Zn anodes inevitably leads to the formation of dendrites, the search for new anode materials for pseudocapacitive storage of Zn ions is also a future research direction.

## Exploitation of the electrolyte

Organic electrolytes are effective at broadening electrochemical windows but are limited by safety issues. The design of an “organic in water” electrolyte should be considered in subsequent studies to address safety issues. WiSs with wide electrochemical windows reduces the binding of Zn ions and water molecules through a solvation effect, which may lead to the development of dendrite-free Zn anodes. However, the high salt concentrations also pose the problems of high cost and increased viscosity of the electrolyte, which limit the rates of ZHSCs. Gel electrolytes or solid electrolytes are cost-effective and environmentally friendly alternatives that provide ion movement channels and offer different functions depending on the composition, such as freezing resistance and self-healing effects. However, it should be noted that new functions should not be designed at the expense of the ionic conductivities, mechanical strengths, etc., of gel electrolytes or solid electrolytes.

## Acknowledgements

The authors gratefully acknowledge the financial support from the National Key R & D Program of China (2021YFB2400400), the National Natural Science Foundation Committee of China (52073143, Key Project of 52131306), and the Project on Carbon Emission Peak and Neutrality of Jiangsu Province (BE2022031-4).

## Author details

<sup>1</sup>School of Energy and Environment, Southeast University, 210096 Nanjing, China. <sup>2</sup>Center for Advancing Electronics Dresden, Technische Universität Dresden, 01069 Dresden, Germany. <sup>3</sup>Hunan Bolt Power New Energy Co. Ltd., Dianjiangjun Industrial Park, Louxing District, 417000 Loudi, Hunan Province, China

## Author contributions

Y.W. conceived and designed the study. X.X. and B.S. reviewed the literature and edited the references. W.F. wrote the manuscript and prepared the figures. W.F., F.W. and Y.W. reviewed and revised the writing. T.W., X.C., Z.Z., and Y.L. reviewed the writing.

## Conflict of interest

The authors declare no competing interests.

**Publisher's note**

Springer Nature remains neutral with regard to jurisdictional claims in published maps and institutional affiliations.

Received: 11 October 2022 Revised: 8 January 2024 Accepted: 22 January 2024

Published online: 05 April 2024

**References**

- Ling, C. A review of the recent progress in battery informatics. *NPJ Comput. Mater.* **8**, 33 (2022).
- Wang, Z. et al. Recent progress of flexible aqueous multivalent ion batteries. *Carbon Energy* **4**, 411–445 (2022).
- Zeng, Y. et al. Recent progress in advanced flexible zinc ion battery design. *Appl. Phys. Rev.* **9**, 021304 (2022).
- Wang, H., Ye, W., Yang, Y., Zhong, Y. & Hu, Y. Zn-ion hybrid supercapacitors: achievements, challenges and future perspectives. *Nano Energy* **85**, 105942 (2021).
- Huang, Z. et al. Recent advances and future perspectives for aqueous zinc-ion capacitors. *Mater. Futures* **1**, 022101 (2022).
- Wang, C., Zeng, X., Cullen, P. J. & Pei, Z. The rise of flexible zinc-ion hybrid capacitors: advances, challenges, and outlooks. *J. Mater. Chem. A* **9**, 19054–19082 (2021).
- Dong, L. et al. Extremely safe, high-rate and ultralong-life zinc-ion hybrid supercapacitors. *Energy Stor. Mater.* **13**, 96–102 (2018).
- Wang, H., Wang, M. & Tang, Y. A novel zinc-ion hybrid supercapacitor for long-life and low-cost energy storage applications. *Energy Stor. Mater.* **13**, 1–7 (2018).
- Shi, Y. et al. An overview and future perspectives of rechargeable zinc batteries. *Small* **16**, e2000730 (2020).
- Chen, D., Lu, M., Cai, D., Yang, H. & Han, W. Recent advances in energy storage mechanism of aqueous zinc-ion batteries. *J. Energy Chem.* **54**, 712–726 (2021).
- He, P. & Huang, J. Detrimental effects of surface imperfections and unpolished edges on the cycling stability of a zinc foil anode. *ACS Energy Lett.* **6**, 1990–1995 (2021).
- Hu, W. et al. Recent progress in tackling Zn anode challenges for Zn ion batteries. *J. Mater. Chem. A* **9**, 25750–25772 (2021).
- Naveed, A. et al. Addressing thermodynamic instability of Zn anode: classical and recent advancements. *Energy Stor. Mater.* **44**, 206–230 (2022).
- Zeng, S. et al. Molten salt assisted synthesis of pitch derived carbon for Zn ion hybrid supercapacitors. *Mater. Res. Bull.* **135**, 111134 (2021).
- Fan, H. et al. Hydrogen-bonded frameworks crystals-assisted synthesis of flower-like carbon materials with penetrable meso/macropores from heavy fraction of bio-oil for Zn-ion hybrid supercapacitors. *J. Colloid Interface Sci.* **600**, 681–690 (2021).
- Liu, P. et al. Mesoporous hollow carbon spheres boosted, integrated high performance aqueous Zn-ion energy storage. *Energy Stor. Mater.* **25**, 858–865 (2020).
- Wei, F., Zhang, H. F., Wang, J. F., Zhuang, J. L. & Lv, Y. H. N, S co-doped porous carbons with well-developed pores for supercapacitor and zinc ion hybrid capacitor. *J. Alloy. Compd.* **907**, 164536 (2022).
- Li, J. et al. Dual-doped carbon hollow nanospheres achieve boosted pseudocapacitive energy storage for aqueous zinc ion hybrid capacitors. *Energy Stor. Mater.* **42**, 705–714 (2021).
- Wang, K. et al. Plasma boosted N, P, O co-doped carbon microspheres for high performance Zn ion hybrid supercapacitors. *J. Alloy. Compd.* **901**, 163588 (2022).
- Cao, Y. F. et al. Thin-walled porous carbon tile-packed paper for high-rate Zn-ion capacitor cathode. *Chem. Eng. J.* **431**, 133241 (2022).
- Li, H. et al. A zinc ion hybrid capacitor based on sharpened pencil-like hierarchically porous carbon derived from metal–organic framework. *Chem. Eng. J.* **428**, 131071 (2022).
- Shao, Y. et al. Regulating oxygen substituents with optimized redox activity in chemically reduced graphene oxide for aqueous Zn-ion hybrid capacitor. *Adv. Funct. Mater.* **31**, 2007843 (2020).
- Dong, L. et al. High-power and ultralong-life aqueous zinc-ion hybrid capacitors based on pseudocapacitive charge storage. *Nanomicro Lett.* **11**, 94 (2019).
- Liu, N. et al. Recent advances and perspectives on vanadium- and manganese-based cathode materials for aqueous zinc ion batteries. *J. Energy Chem.* **59**, 134–159 (2021).
- Ma, X. et al. Multivalent ion storage towards high-performance aqueous zinc-ion hybrid supercapacitors. *Energy Storage Mater.* **20**, 335–342 (2019).
- Wang, S. et al. A new free-standing aqueous zinc-ion capacitor Based on MnO<sub>2</sub>-CNTs cathode and MXene anode. *Nanomicro Lett.* **11**, 70 (2019).
- Li, Q. et al. Co<sub>9</sub>S<sub>8</sub>@MnO<sub>2</sub> core-shell defective heterostructure for High-Voltage flexible supercapacitor and Zn-ion hybrid supercapacitor. *Chem. Eng. J.* **437**, 135494 (2022).
- Chen, Q. et al. Zn<sup>2+</sup> pre-intercalation stabilizes the tunnel structure of MnO<sub>2</sub> nanowires and enables zinc-ion hybrid supercapacitor of battery-level energy density. *Small* **16**, e2000091 (2020).
- Li, X. et al. A flexible Zn-ion hybrid micro-supercapacitor based on MXene anode and V<sub>2</sub>O<sub>5</sub> cathode with high capacitance. *Chem. Eng. J.* **428**, 130965 (2022).
- Yang, Q. et al. A wholly degradable, rechargeable Zn-Ti<sub>3</sub>C<sub>2</sub> MXene capacitor with superior anti-self-discharge function. *ACS Nano* **13**, 8275–8283 (2019).
- Chen, J. et al. Nacre-inspired surface-engineered MXene/nanocellulose composite film for high-performance supercapacitors and zinc-ion capacitors. *Chem. Eng. J.* **428**, 131380 (2022).
- Chen, J. et al. Simplified synthesis of fluoride-free Ti<sub>3</sub>C<sub>2</sub>T<sub>x</sub> via electrochemical etching toward high-performance electrochemical capacitors. *ACS Nano* **16**, 2461–2470 (2022).
- Fan, Z. et al. 3D-printed Zn-ion hybrid capacitor enabled by universal divalent cation-gelated additive-free Ti<sub>3</sub>C<sub>2</sub> MXene Ink. *ACS Nano* **15**, 3098–3107 (2021).
- Jin, Y. et al. A high-rate, long life, and anti-self-discharge aqueous N-doped Ti<sub>3</sub>C<sub>2</sub>/Zn hybrid capacitor. *Mater. Today Energy* **19**, 100598 (2021).
- Li, F. et al. 3D porous H-Ti<sub>3</sub>C<sub>2</sub>T<sub>x</sub> films as free-standing electrodes for zinc ion hybrid capacitors. *Chem. Eng. J.* **435**, 135052 (2022).
- Li, X. et al. Vertically aligned Sn<sub>4+</sub> preintercalated Ti<sub>3</sub>CT<sub>x</sub> MXene sphere with enhanced Zn ion transportation and superior cycle lifespan. *Adv. Energy Mater.* **10**, 2001394 (2020).
- Zhang, W. et al. Pizza-like heterostructured Ti<sub>3</sub>C<sub>2</sub>T<sub>x</sub>-Bi<sub>2</sub>S<sub>3</sub>@N-C with ultra-high specific capacitance as a potential electrode material for aqueous zinc-ion hybrid supercapacitors. *J. Alloy. Compd.* **883**, 160881 (2021).
- Huang, C. et al. Sewable and cuttable flexible zinc-ion hybrid supercapacitor using a polydopamine/carbon cloth-based cathode. *ACS Sustain. Chem. Eng.* **8**, 16028–16036 (2020).
- Wang, W. et al. Phenanthroline covalent organic framework electrodes for high-performance zinc-ion supercapattery. *ACS Energy Lett.* **5**, 2256–2264 (2020).
- Xin, T. et al. A high-capacity aqueous Zn-ion hybrid energy storage device using poly(4,4'-thiodiphenol)-modified activated carbon as a cathode material. *J. Mater. Chem. A* **7**, 23076–23083 (2019).
- Guo, Q., Han, Y., Chen, N. & Qu, L. Few-layer siloxene as an electrode for superior high-rate zinc ion hybrid capacitors. *ACS Energy Lett.* **6**, 1786–1794 (2021).
- Huang, Z. et al. Phosphorene as cathode material for high-voltage, anti-self-discharge zinc ion hybrid capacitors. *Adv. Energy Mater.* **10**, 2001024 (2020).
- Huang, Z. et al. Effects of anion carriers on capacitance and self-discharge behaviors of zinc ion capacitors. *Angew. Chem. Int. Ed. Engl.* **60**, 1011–1021 (2021).
- Hao, J. et al. Deeply understanding the Zn anode behaviour and corresponding improvement strategies in different aqueous Zn-based batteries. *Energy Environ. Sci.* **13**, 3917–3949 (2020).
- Wang, X. et al. An aqueous rechargeable Zn//Co<sub>3</sub>O<sub>4</sub> battery with high energy density and good cycling behavior. *Adv. Mater.* **28**, 4904–4911 (2016).
- Xiao, R. et al. Localizing concentrated electrolyte in pore geometry for highly reversible aqueous Zn metal batteries. *Chem. Eng. J.* **420**, 129642 (2021).
- Qian, Y., Meng, C., He, J. & Dong, X. A lightweight 3D Zn@Cu nanosheet-s@activated carbon cloth as long-life anode with large capacity for flexible zinc ion batteries. *J. Power Sources* **480**, 228871 (2020).
- Xu, Z. et al. Efficient Zn metal anode enabled by O,N-codoped carbon microflowers. *Nano Lett.* **22**, 1350–1357 (2022).
- Wang, Z. et al. A metal-organic framework host for highly reversible dendrite-free zinc metal anodes. *Joule* **3**, 1289–1300 (2019).
- An, G. H. et al. 2D metal Zn nanostructure electrodes for high-performance Zn ion supercapacitors. *Adv. Energy Mater.* **10**, 1902981 (2019).

51. Kwon, M. et al. Stimulating Cu–Zn alloying for compact Zn metal growth towards high energy aqueous batteries and hybrid supercapacitors. *Energy Environ. Sci.* **15**, 2889–2899 (2022).
52. Tao, H., Hou, Z., Zhang, L., Yang, X. & Fan, L.-Z. Manipulating alloying reaction to achieve the stable and dendrite-free zinc metal anodes. *Chem. Eng. J.* **450**, 138048 (2022).
53. Chen, P. et al. An artificial polyacrylonitrile coating layer confining zinc dendrite growth for highly reversible aqueous zinc-based batteries. *Adv. Sci.* **8**, 2100309 (2021).
54. Cao, Z. et al. Eliminating Zn dendrites by commercial cyanoacrylate adhesive for zinc ion battery. *Energy Stor. Mater.* **36**, 132–138 (2021).
55. Yan, H., Li, S., Nan, Y., Yang, S. & Li, B. Ultrafast zinc-ion–conductor interface toward high-rate and stable zinc metal batteries. *Adv. Energy Mater.* **11**, 2100186 (2021).
56. Niu, B. et al. Robust Zn anode enabled by a hydrophilic adhesive coating for long-life zinc-ion hybrid supercapacitors. *Chem. Eng. J.* **442**, 136217 (2022).
57. Cui, M. et al. A new flexible porous protective layers with high binding strength for stable Zn anodes. *Chem. Eng. J.* **434**, 134688 (2022).
58. Long, Y. et al. In-situ regulation of zinc metal surface for Dendrite-Free Zinc-ion hybrid supercapacitors. *J. Colloid Interface Sci.* **614**, 205–213 (2022).
59. Zou, K. et al. Highly stable zinc metal anode enabled by oxygen functional groups for advanced Zn-ion supercapacitors. *Chem. Commun.* **57**, 528–531 (2021).
60. Fan, W. et al. High cycle stability of Zn anodes boosted by an artificial electronic–ionic mixed conductor coating layer. *J. Mater. Chem. A* **10**, 7645–7652 (2022).
61. Li, C., Jin, S., Archer, L. A. & Nazar, L. F. Toward practical aqueous zinc-ion batteries for electrochemical energy storage. *Joule* **6**, 1733–1738 (2022).
62. Shi, J. et al. A new flexible zinc-ion capacitor based on  $\delta$ -MnO<sub>2</sub>@Carbon cloth battery-type cathode and MXene@Cotton cloth capacitor-type anode. *J. Power Sources* **446**, 227345 (2020).
63. Wen, L. et al. A novel TiSe<sub>2</sub> (de)intercalation type anode for aqueous zinc-based energy storage. *Nano Energy* **93**, 106896 (2022).
64. Yu, M. et al. A high-rate two-dimensional polyarylimide covalent organic framework anode for aqueous Zn-ion energy storage devices. *J. Am. Chem. Soc.* **142**, 19570–19578 (2020).
65. Cui, F.-Z. et al. Polyarylimide and porphyrin based polymer microspheres for zinc ion hybrid capacitors. *Chem. Eng. J.* **405**, 127038 (2021).
66. Zhou, H. et al. Boosting the electrochemical performance through proton transfer for the Zn-ion hybrid supercapacitor with both ionic liquid and organic electrolytes. *J. Mater. Chem. A* **7**, 9708–9715 (2019).
67. Zhang, L., Liu, Z., Wang, G., Feng, J. & Ma, Q. Developing high voltage Zn(TFSI)<sub>2</sub>/Py<sub>14</sub>TFSI/AN hybrid electrolyte for a carbon-based Zn-ion hybrid capacitor. *Nanoscale* **13**, 17068–17076 (2021).
68. Zhang, L. et al. Designing a Zn(BF<sub>4</sub>)<sub>2</sub>-based ionic liquid electrolyte to realize superior energy density in a carbon-based zinc-ion hybrid capacitor. *ChemElectroChem* **8**, 1289–1297 (2021).
69. Qiu, X., Wang, N., Wang, Z., Wang, F. & Wang, Y. Towards high-performance zinc-based hybrid supercapacitors via macropores-based charge storage in organic electrolytes. *Angew. Chem. Int. Ed. Engl.* **60**, 9610–9617 (2021).
70. Wang, C. et al. Toward flexible zinc-ion hybrid capacitors with superhigh energy density and ultralong cycling life: the pivotal role of ZnCl<sub>2</sub> salt-based electrolytes. *Angew. Chem. Int. Ed. Engl.* **60**, 990–997 (2021).
71. Gavriel, B. et al. Enhanced performance of Ti<sub>3</sub>C<sub>2</sub>T<sub>x</sub> (MXene) electrodes in concentrated ZnCl<sub>2</sub> solutions: a combined electrochemical and EQCM-D study. *Energy Stor. Mater.* **38**, 535–541 (2021).
72. Han, J. et al. Zinc-ion hybrid supercapacitors employing acetate-based water-in-salt electrolytes. *Small* **18**, e2201563 (2022).
73. Han, L. et al. Novel zinc–iodine hybrid supercapacitors with a redox iodide ion electrolyte and B, N dual-doped carbon electrode exhibit boosted energy density. *J. Mater. Chem. A* **7**, 24400–24407 (2019).
74. Han, L. et al. A novel redox bromide-ion additive hydrogel electrolyte for flexible Zn-ion hybrid supercapacitors with boosted energy density and controllable zinc deposition. *J. Mater. Chem. A* **8**, 15042–15050 (2020).
75. Yu, F. et al. A zinc bromine “supercapattery” system combining triple functions of capacitive, pseudocapacitive and battery-type charge storage. *Mater. Horiz.* **7**, 495–503 (2020).
76. Zhou, Z. et al. In situ two-step activation strategy boosting hierarchical porous carbon cathode for an aqueous Zn-based hybrid energy storage device with high capacity and ultra-long cycling life. *Small* **16**, e2003174 (2020).
77. Zhang, H. et al. Boosting Zn-ion energy storage capability of hierarchically porous carbon by promoting chemical adsorption. *Adv. Mater.* **31**, 1904948 (2019).
78. Zhang, X. et al. Flexible zinc-ion hybrid fiber capacitors with ultrahigh energy density and long cycling life for wearable electronics. *Small* **15**, e1903817 (2019).
79. Chen, S. et al. A flexible solid-state zinc ion hybrid supercapacitor based on co-polymer derived hollow carbon spheres. *J. Mater. Chem. A* **7**, 7784–7790 (2019).
80. Shi, B. et al. Continuous fabrication of Ti<sub>3</sub>C<sub>2</sub>T<sub>x</sub> MXene-based braided coaxial zinc-ion hybrid supercapacitors with improved performance. *Nanomicro Lett.* **14**, 34 (2021).
81. Lu, Y. et al. High energy-power Zn-ion hybrid supercapacitors enabled by layered B/N co-doped carbon cathode. *Nano Energy* **66**, 104132 (2019).
82. Yang, H. et al. A supramolecular gel polymer electrolyte for ultralong-life zinc-ion hybrid supercapacitors. *J. Energy Storage* **53**, 105089 (2022).
83. Huang, H. et al. A powder self-healable hydrogel electrolyte for flexible hybrid supercapacitors with high energy density and sustainability. *Small* **17**, e2006807 (2021).
84. Zhu, X. et al. Freeze-tolerant hydrogel electrolyte with high strength for stable operation of flexible zinc-ion hybrid supercapacitors. *Small* **18**, e2200055 (2022).
85. Liu, J. et al. Flexible antifreeze Zn-ion hybrid supercapacitor based on gel electrolyte with graphene electrodes. *ACS Appl. Mater. Interfaces* **13**, 16454–16468 (2021).
86. Li, F. et al. Fabricating low-temperature-tolerant and durable Zn-ion capacitors via modulation of co-solvent molecular interaction and cation solvation. *Sci. China Mater.* **64**, 1609–1620 (2021).
87. Liu, J., Ahmed, S., Wang, T. & Song, S. flexible thermotolerant Zn-ion hybrid supercapacitors enabled by heat-resistant polymer electrolyte. *Chem. Eng. J.* **451**, 138512 (2023).
88. Wang, J., Li, F., Zhu, F. & Schmidt, O. G. Recent progress in micro-supercapacitor design, integration, and functionalization. *Small Methods* **3**, 1800367 (2018).
89. Zeng, J. et al. Printable zinc-ion hybrid micro-capacitors for flexible self-powered integrated units. *Nanomicro Lett.* **13**, 19 (2020).
90. Tian, W. et al. Implantable and biodegradable micro-supercapacitor based on a superassembled three-dimensional network Zn@PPy hybrid electrode. *ACS Appl. Mater. Interfaces* **13**, 8285–8293 (2021).
91. Li, L. et al. In-situ annealed Ti<sub>3</sub>C<sub>2</sub>T<sub>x</sub> MXene based all-solid-state flexible Zn-ion hybrid micro supercapacitor array with enhanced stability. *Nanomicro Lett.* **13**, 100 (2021).
92. Zhang, P. et al. Zn-ion hybrid micro-supercapacitors with ultrahigh areal energy density and long-term durability. *Adv. Mater.* **31**, 1806005 (2019).
93. Cao, Z., Fu, J., Wu, M., Hua, T. & Hu, H. Synchronously manipulating Zn<sup>2+</sup> transfer and hydrogen/oxygen evolution kinetics in MXene host electrodes toward symmetric Zn-ions micro-supercapacitor with enhanced areal energy density. *Energy Stor. Mater.* **40**, 10–21 (2021).
94. Cao, Z., Hu, H. & Ho, D. Micro-redoxcapacitor: a hybrid architecture out of the notorious energy-power density dilemma. *Adv. Funct. Mater.* **32**, 2111805 (2022).
95. Sun, G. et al. A capacity recoverable zinc-ion micro-supercapacitor. *Energy Environ. Sci.* **11**, 3367–3374 (2018).
96. Wang, X. et al. Flexible energy-storage devices: design consideration and recent progress. *Adv. Mater.* **26**, 4763–4782 (2014).
97. Yan, Y., Liu, X., Yan, J., Guan, C. & Wang, J. Electrospun nanofibers for new generation flexible energy storage. *Energy Environ. Mater.* **4**, 502–521 (2021).
98. Ni, T. et al. Highly flexible and self-healable zinc-ion hybrid supercapacitors based on MWCNTs-RGO fibers. *Adv. Mater. Technol.* **5**, 2000268 (2020).
99. Pu, J. et al. Ultrafast-charging quasi-solid-state fiber-shaped zinc-ion hybrid supercapacitors with superior flexibility. *J. Mater. Chem. A* **9**, 17292–17299 (2021).
100. Wang, H., Chen, Q., Xiao, P. & Cao, L. Unlocking zinc-ion energy storage performance of onion-like carbon by promoting heteroatom doping strategy. *ACS Appl. Mater. Interfaces* **14**, 9013–9023 (2022).
101. Zhao, J. et al. Regulating zinc electroplating chemistry to achieve high energy coaxial fiber Zn ion supercapacitor for self-powered textile-based monitoring system. *Nano Energy* **93**, 106893 (2022).
102. Boruah, B. D. et al. Photo-rechargeable zinc-ion capacitor using 2D graphitic carbon nitride. *Nano Lett.* **20**, 5967–5974 (2020).

103. Boruah, B. D. et al. Photo-rechargeable zinc-ion capacitors using  $V_2O_5$ -activated carbon electrodes. *ACS Energy Lett.* **5**, 3132–3139 (2020).
104. Ma, L. et al. A usage scenario independent “air chargeable” flexible zinc ion energy storage device. *Adv. Energy Mater.* **9**, 1900509 (2019).
105. Sun, G. et al. Hybrid energy storage device: combination of zinc-ion supercapacitor and zinc–air battery in mild electrolyte. *ACS Appl. Mater. Interfaces* **12**, 7239–7248 (2020).
106. Yang, L. et al. Self-chargeable zinc-ion hybrid supercapacitor driven by salt-concentrated cellulose hydrogel. *Cellulose* **28**, 11483–11492 (2021).
107. Chen, M., Chen, J., Zhou, W., Xu, J. & Wong, C.-P. High-performance flexible and self-healable quasi-solid-state zinc-ion hybrid supercapacitor based on borax-crosslinked polyvinyl alcohol/nanocellulose hydrogel electrolyte. *J. Mater. Chem. A* **7**, 26524–26532 (2019).
108. Chen, Q., Zhao, J., Chen, Z., Jin, Y. & Chen, J. High voltage and self-healing zwitterionic double-network hydrogels as electrolyte for zinc-ion hybrid supercapacitor/battery. *Int. J. Hydrog. Energy* **47**, 23909–23918 (2022).
109. Ji, G., Hu, R., Wang, Y. & Zheng, J. High energy density, flexible, low temperature resistant and self-healing Zn-ion hybrid capacitors based on hydrogel electrolyte. *J. Energy Storage* **46**, 103858 (2022).
110. Wang, Q. et al. Mxene-reduced graphene oxide aerogel for aqueous zinc-ion hybrid supercapacitor with ultralong cycle life. *Adv. Electron. Mater.* **5**, 1900537 (2019).
111. Huang, L. et al. Highly transparent and flexible  $Zn-Ti_3C_2T_x$  MXene hybrid capacitors. *Langmuir* **38**, 5968–5976 (2022).